NPS ARCHIVE
1959
BLADES, L.

# AN ANALYSIS OF A DIGITAL SAMPLED DATA SERVOMECHANISM AND THE DESIGN OF A SWITCHING DEVICE FOR DUAL MODE OPERATION

---

LAWRENCE T. BLADES

DUDLEY KNOX LIBRARY
NAVAL POSTGRADUATE SCHOOL
MONTEREY, CA 93943-5101

LIBRARY
U.S. NAVAL POSTGRADUATE SCHOOL
MONTEREY, CALIFORNIA

DUDLEY KNOX LIBRARY
NAVAL POSTGRADUATE SCHOOL
MONTEREY, CA 93943-5101

# AN ANALYSIS OF A DIGITAL SAMPLED DATA SERVOMECHANISM

# AND THE

# DESIGN OF A SWITCHING DEVICE FOR DUAL MODE OPERATION

* * * * *

Lawrence T. Blades

# AN ANALYSIS OF A DIGITAL SAMPLED DATA SERVOMECHANISM

# AND THE

# DESIGN OF A SWITCHING DEVICE FOR DUAL MODE OPERATION


by

Lawrence T. Blades

Lieutenant, United States Navy


Submitted in partial fulfillment of
the requirements for the degree of

MASTER OF SCIENCE
IN
ELECTRICAL ENGINEERING


United States Naval Postgraduate School
Monterey, California

1959

NPS ARCHIVE
1959
BLADES, L.

Thesis
B5458

DUDLEY KNOX LIBRARY
NAVAL POSTGRADUATE SCHOOL
MONTEREY, CA 93943-5101

# AN ANALYSIS OF A DIGITAL SAMPLED DATA SERVOMECHANISM AND THE DESIGN OF A SWITCHING DEVICE FOR DUAL MODE OPERATION

by

Lawrence T. Blades

This work is accepted as fulfilling
the thesis requirements for the degree of
MASTER OF SCIENCE
IN
ELECTRICAL ENGINEERING
from the
United States Naval Postgraduate School

ABSTRACT

Digital automatic control systems operating on sampled data have become more widely used in recent years to take advantage of the versatility and accuracy of digital computers, and new servomechanism compensation techniques utilizing digital devices are being developed for use in these systems. The present paper is an analysis of a particular digital control system, its response to large step inputs which cause plant saturation, and the design of a simple switching device for dual mode operation which takes advantage of digital logic circuitry.

The author wishes to express his appreciation for the assistance given him by the engineers and technicians of the Servomechanisms Section of Philco Corporation, Western Development Laboratories, Palo Alto, California where this work was carried on, in particular to Mr. Lynn J. Harvey, Mr. Joseph L. Heim, and Dr. Gene F. Franklin of Stanford University, a Philco Consultant. He wishes to express his appreciation also for the assistance rendered him by Lieutenant Thomas C. Warren, U.S. Navy, and to Professor George J. Thaler, Dr. Eng., faculty advisor.

TABLE OF CONTENTS

## LIST OF ILLUSTRATIONS

| Figures | | Page |
|---|---|---|

## LIST OF TABLES

# I INTRODUCTION

In recent years, with the advent of space satellites, there has been an increased emphasis on the development of extremely accurate positioning servomechanisms necessary in satellite tracking and directional telemetry receiving systems. A method of accomplishing this extreme accuracy involves the use of digital servomechanisms employing analog-to-digital shaft position encoders to gain the high positioning accuracy.

In a particular application under development at Philco Corporation, Western Development Laboratories, a positioning servomechanism uses a disc-type analog-to-digital converter capable of reading $2^{16}$ shaft positions or, stated another way, capable of resolution to one part in 65,536. The particular converter being used is a photo-electric device using a flashing light source to activate photocells for digital readout, and as such, makes the servo a sampled data system. The system uses a digital input signal from a digital computer, and uses a hydraulic power source.

During the period that the work of the present paper was undertaken by the author, June and July, 1959, the system was inherently velocity limited, and it was desired that further analysis of the system be made with a view to raising the maximum velocity obtainable if possible.

An experimental model of the servomechanism had been made,

employing, however, a two-phase, 60cycle a-c servomotor as a prime mover instead of the hydraulic plant, and the present investigation was carried out on this model system.

## II GENERAL DESCRIPTION OF THE SERVOMECHANISM AND ITS MAJOR COMPONENT PARTS

### 2.1 Introduction

In Figure 1 is shown the experimental model of the digital sampled data servomechanism which was used in this investigation. In Figure 2 is shown a functional block diagram of the model indicating the function each component plays in the servomechanism loop. The remaining articles in this section are brief physical descriptions of these component parts.

### 2.2 Baldwin, Model A9SP16, 16 Digit Photoelectric Analog-to-Digital Shaft Position Encoder

Reference (1) contains a basic description of this device. This shaft position converter is a device which gives an indication of shaft position in digital form. Basically, it makes use of a disc divided into 16 concentric zones, each zone representing a binary digit. The least significant digit zone is at the periphery of the disc with more significant digit zones displaced toward the center. The disc is made of glass, and each digit zone or ring is divided into clear and opaque segments, the angular span of each segment being determined by the significance of the digit represented by the ring. In particular, since this is a 16 digit encoder, the disc "sees" $2^{16}$ or 65,536 positions per revolution. Thus, in the least significant zone of the disc there are 65,536 opaque and a like number of clear segments.

The coded disc is integrally mounted to the shaft being encoded. Readout of position is performed by photocells,

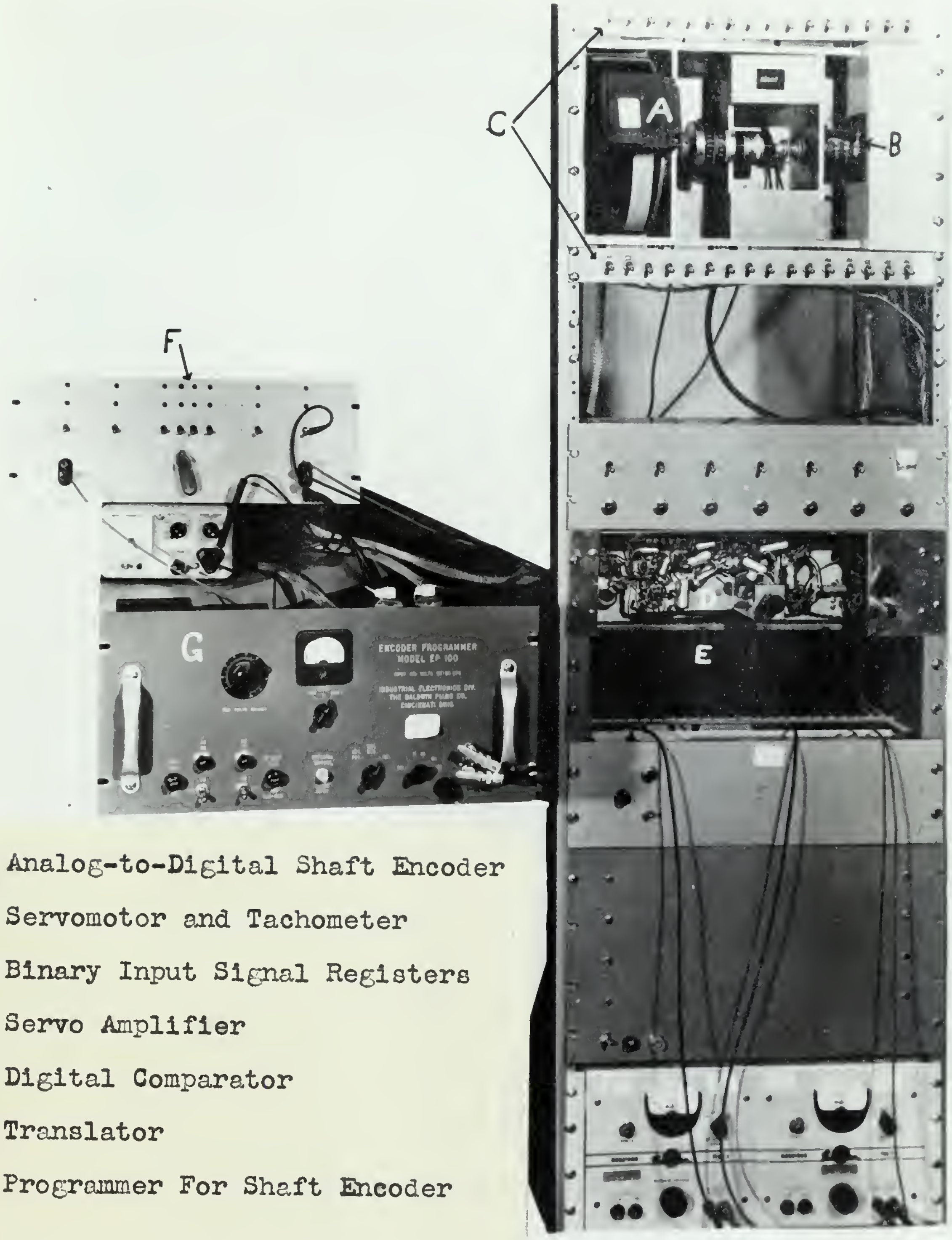


A Analog-to-Digital Shaft Encoder

B Servomotor and Tachometer

C Binary Input Signal Registers

D Servo Amplifier

E Digital Comparator

F Translator

G Programmer For Shaft Encoder

Figure 1. Experimental Model of a Digital Sampled Data Position Servomechanism

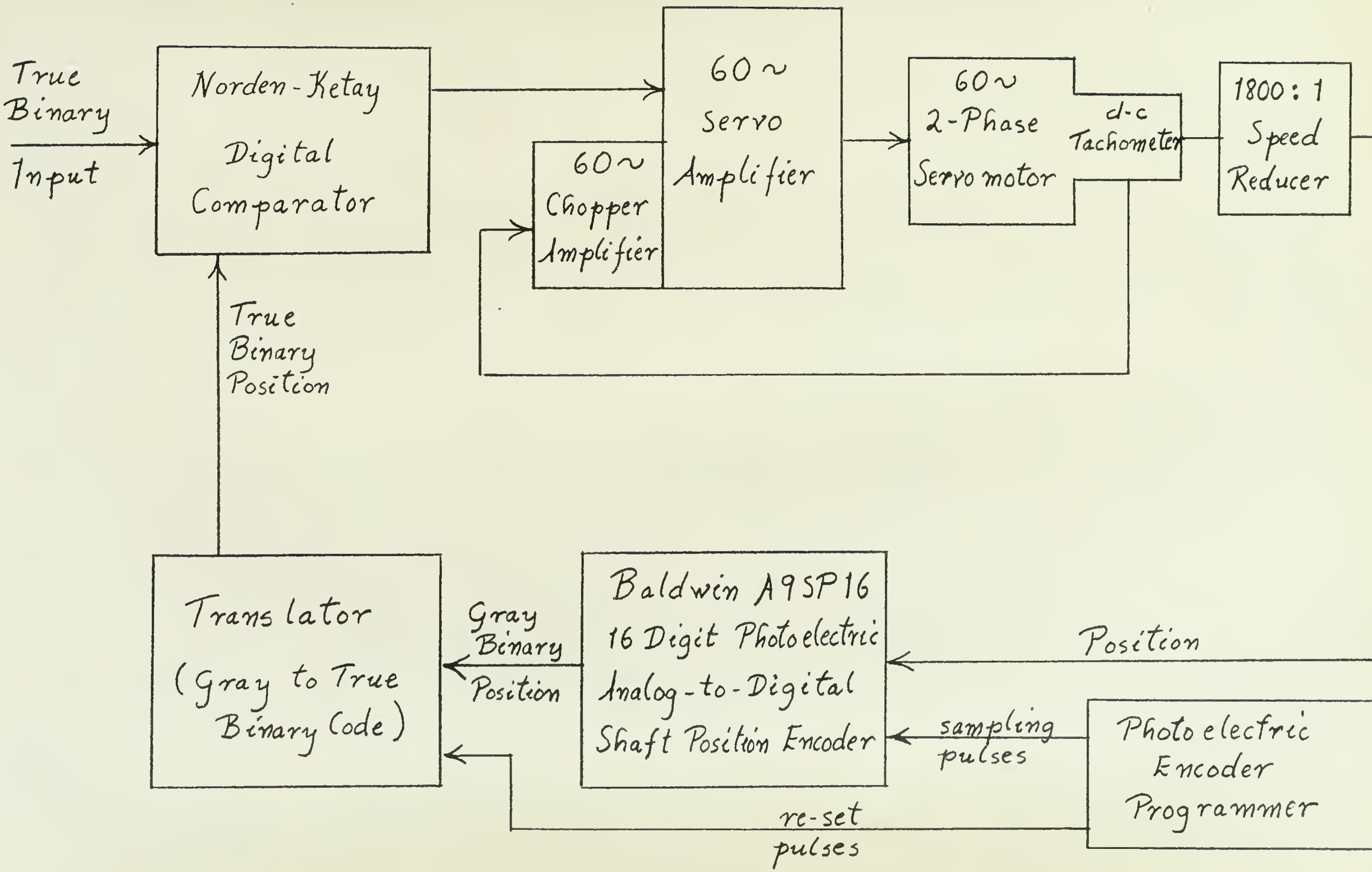


Figure 2. Functional Block Diagram of a Digital Sampled Data Position Servo.

activated by a flashing light. Figure 3 shows functionally how this is done. When the lamp is triggered, light passing through the code disc is read by a bank of radially positioned photocells, one for each ring on the code disc, that is, one for each digit. Clear sectors of the disc give a "1" output, while opaque sectors give a "0" output. As the shaft rotates, the disc moves integrally with it, while the photocell bank and light source remain fixed as a reference, thus, the binary word output changes.

Since the light source flashes, it is this feature of the encoder which makes the system a sampled data system.

The coding of the disc is not done in true binary. If it were, ambiguities could occur principally because in a true binary counting sequence more than one digit changes at a time, and since the light source and photocells are of finite size, there could be large errors if several zones were changing instantaneously and all of them were not properly read by the photocells. For this reason the disc is encoded in "Gray" Binary Code, named for its inventor, Dr. Frank Gray, which minimizes ambiguities by allowing only one zone to change condition at a time. A description of this code is contained in Appendix I.

Photocell outputs are sent to individual three-stage transistor amplifiers which convert the photocell current pulses into suitable output voltages. This encoder is a so-called "parallel" converter because it transmits all 16 digits simultaneously. Thus, from the encoder output through the

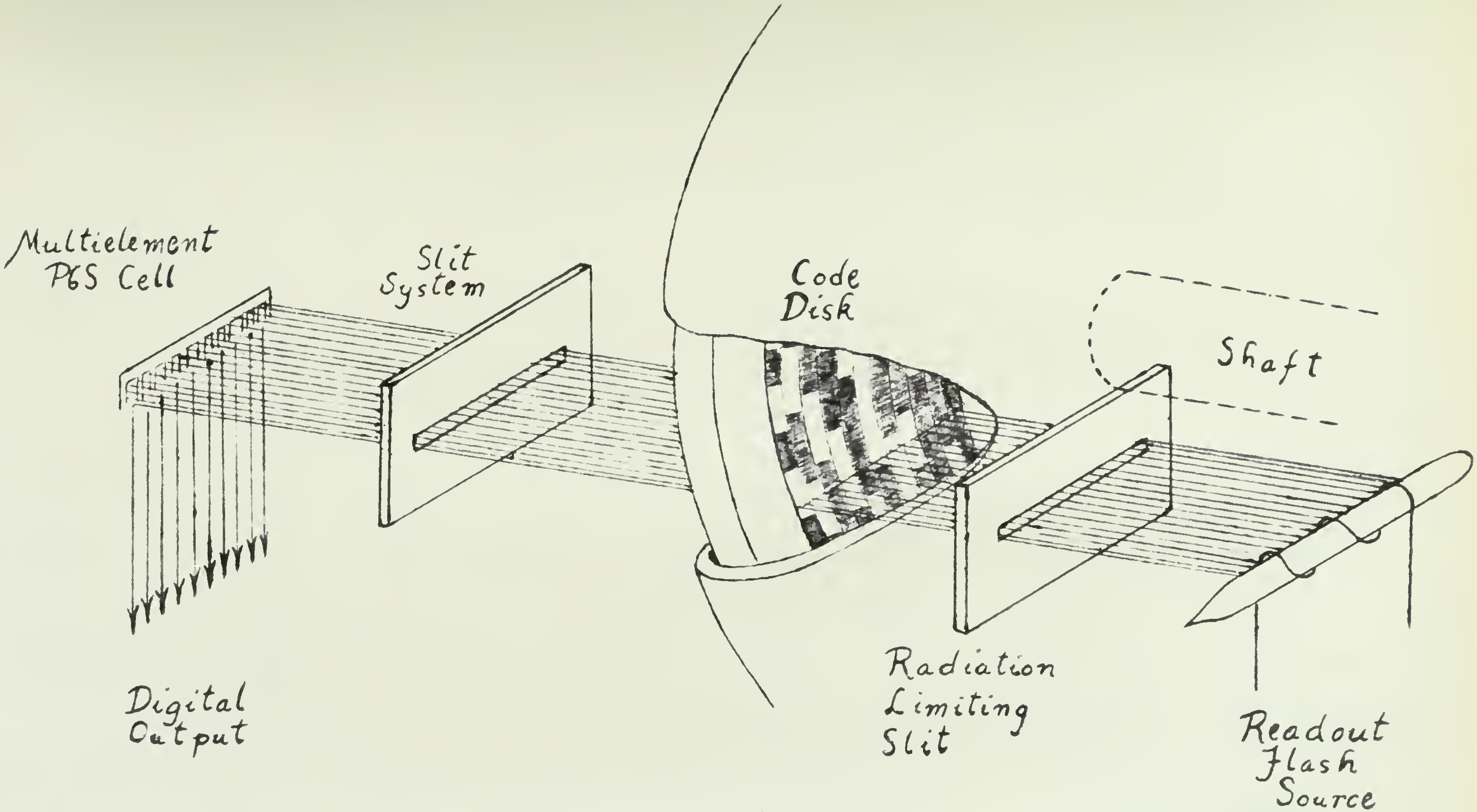


Figure 3. Functional Diagram of Readout System of a Photoelectric Analog-to-Digital Shaft Encoder.

translator and into the digital comparator of Figure 2 there are 16 parallel electrical transmission links.

The encoder programmer, shown in Figure 1 and 2 supplies power and light source timing to the encoder. During this investigation the light timing, or sampling rate, was set at 25 samples per second. This particular rate had been decided upon by the system designers, taking into account time-sharing considerations outside of the system itself.

## 2.3 Translator

The function of this device is the translation of the Gray binary output of the encoder into a natural binary equivalent for input to the comparator. As explained in Appendix I, to convert a Gray binary number to its true binary equivalent, it is necessary to carry the most significant digit unchanged, and then consecutively add digits to the right, the true binary equivalent digit being the result of each addition, as shown by following the arrows in the example below:

| | | | | | | | |
|---|---|---|---|---|---|---|---|
| Gray Number: | 1 | 1 | 1 | 1 | 1 | 0 | 0 |
| True Binary Number: | 1 | 0 | 1 | 0 | 1 | 1 | 1 |

In the translator this is performed electrically as follows: Each of the digit channels from the encoder feeds a separate transistor circuit board in the translator. The most significant digit board has only a flip-flop circuit which is triggered by a pulse from the encoder and it gives

an output signal of proper magnitude for transmission to the comparator. This output also goes to an "and" gate on the next most significant digit board. All the remaining 15 digit boards are identical and consist primarily of a flip-flop circuit and an "and" gate circuit. Each flip-flop receives and "holds" its pulse from the encoder as in the most significant digit case, but now, instead of the flip-flop output going directly to the comparator, it is sent to the "and" gate where it is combined with the output signal of the previous board to produce the true binary digit output to the comparator and to the gate circuit of the next board. On its way to the comparator, the output of each board also activates a light on the front panel of the translator, shown in Figure 1, for output shaft position reading purposes.

The flip-flop circuits are re-set in time to hold the next incoming digit by re-set pulses from the encoder programmer as shown in Figure 2, these re-sets being timed with the sampling pulses.

### 2.4 Norden-Ketay Digital Comparator

The Norden-Ketay Digital Comparator, shown in Figures 1 and 2, and described in reference (2), has as its purpose the comparison of two binary numbers and supplying as an output an a-c, amplitude modulated signal with amplitude and phase being proportional to the difference between the input binary numbers.

Figure 4 is a functional diagram of the comparator. The function of the block marked "Logic Circuits" is to close

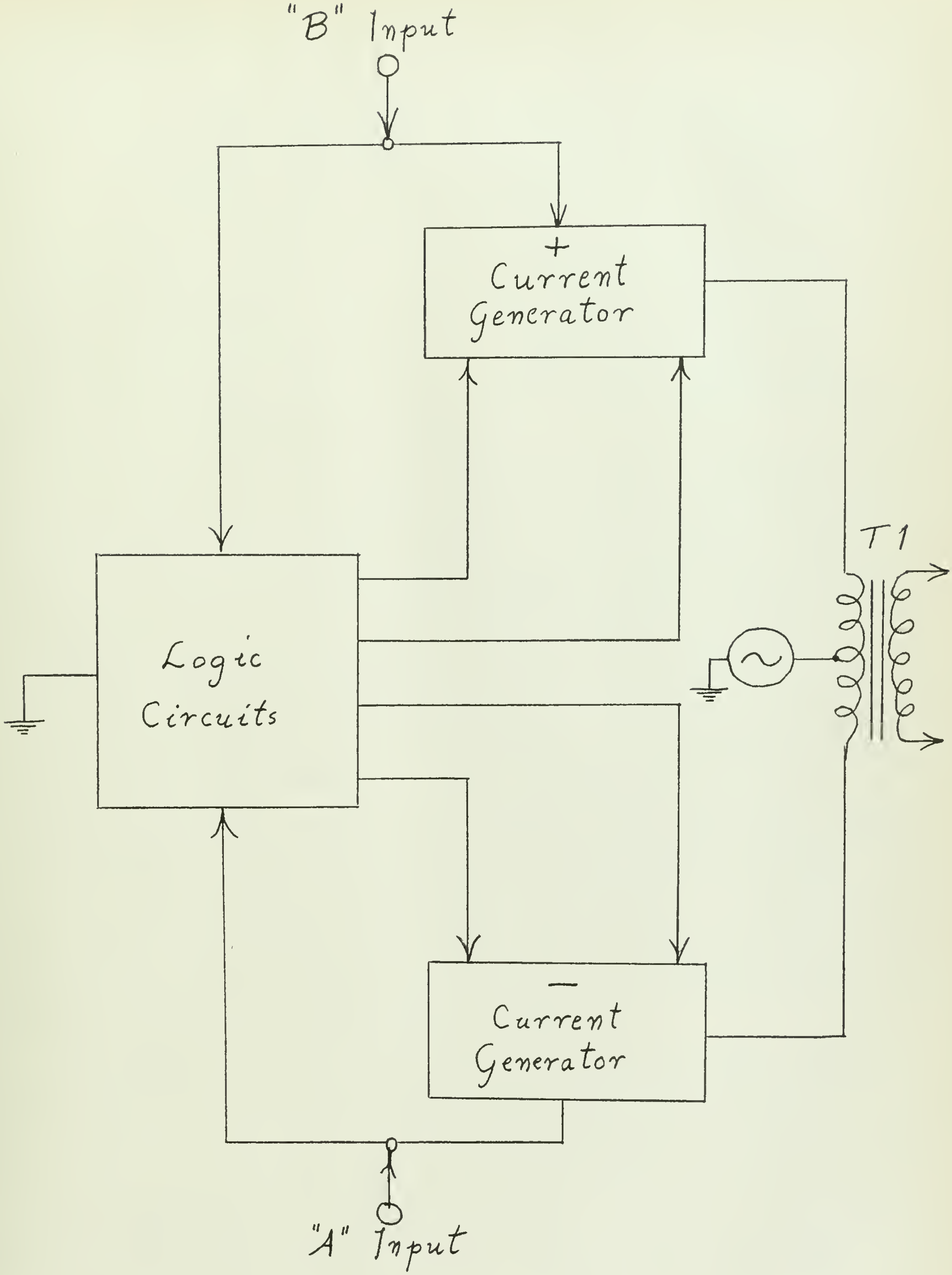


Figure 4. Function Diagram of the Digital Comparator.

combinations of transistor switches in the + and — "Current Generators", thus, producing an a-c output voltage at the output winding of T1 proportional to the difference between the two input numbers. The current generators each consist of six transistors with collector load resistors so weighted that each more significant binary digit or "bit" produces twice as much current as the preceding bit. These two currents are then added in the primary of T1, which is also supplied with a 115 volt, 60 cps a-c line voltage.

The details of the logic circuitry of the comparator are not pertinent to this report and will not be described, other than to say that the design uses "current" logic which is set up to establish a single current path through a number of possible paths. The transistors in the logic section thus may be considered as open or closed switches. Of particular importance to this investigation is the fact that, in order to simplify the design of the logic section, this comparator gives a true voltage analog output proportional to the difference between the two input binary numbers only up to a six digit number from zero to $2^5$ or 32 bits. When the difference is greater than this the output is constant.

The entire comparator is built on a modular basis, using semi-conductors mounted on etched plug-in boards exclusively. In addition to the 115 volt, 60 cps a-c voltage, the device must be supplied with three d-c voltages: + 2 volts, −11 volts, and −13 volts. The logical voltage levels used in the logic

section are:

$$-11 \text{ volts} = "1" = \text{true}$$

$$0 \text{ volts} = "0" = \text{false}.$$

## 2.5 Servo Amplifier

Figure 5 is the circuit diagram of the amplifier used in the model servomechanism. There are two inputs to the amplifier, the 60 cps, amplitude modulated voltage from the comparator output, and the d-c tachometer feedback voltage, as shown in Figure 2. The first two stages are a chopper amplifier where the d-c tachometer voltage is converted to a crude 60 cps a-c by a mechanical chopper, activated by 60 cps line voltage, and this crude a-c is smoothed and amplified in the first two stages, $V_1$ and $V_2$. Note that due to 165K resistor on the chopper input, the d-c voltage from the tachometer is greatly attenuated; in practice, the maximum input was ±20 millivolts. A potentiometer controls the level of the a-c tach voltage forwarded to the remaining stages of the amplifier. Further tach amplification is performed in $V_3$ and $V_5$.

The comparator output signal comes into $V_4$ and is further amplified in $V_6$. Summing of the two signals is performed at the gain potentiometer. The remaining stages amplify the combined signal to produce a push-pull output to the motor control field winding. The .25 mfd capacitor across the output transformer produces the required 90 degree phase shift for the motor control field voltage.

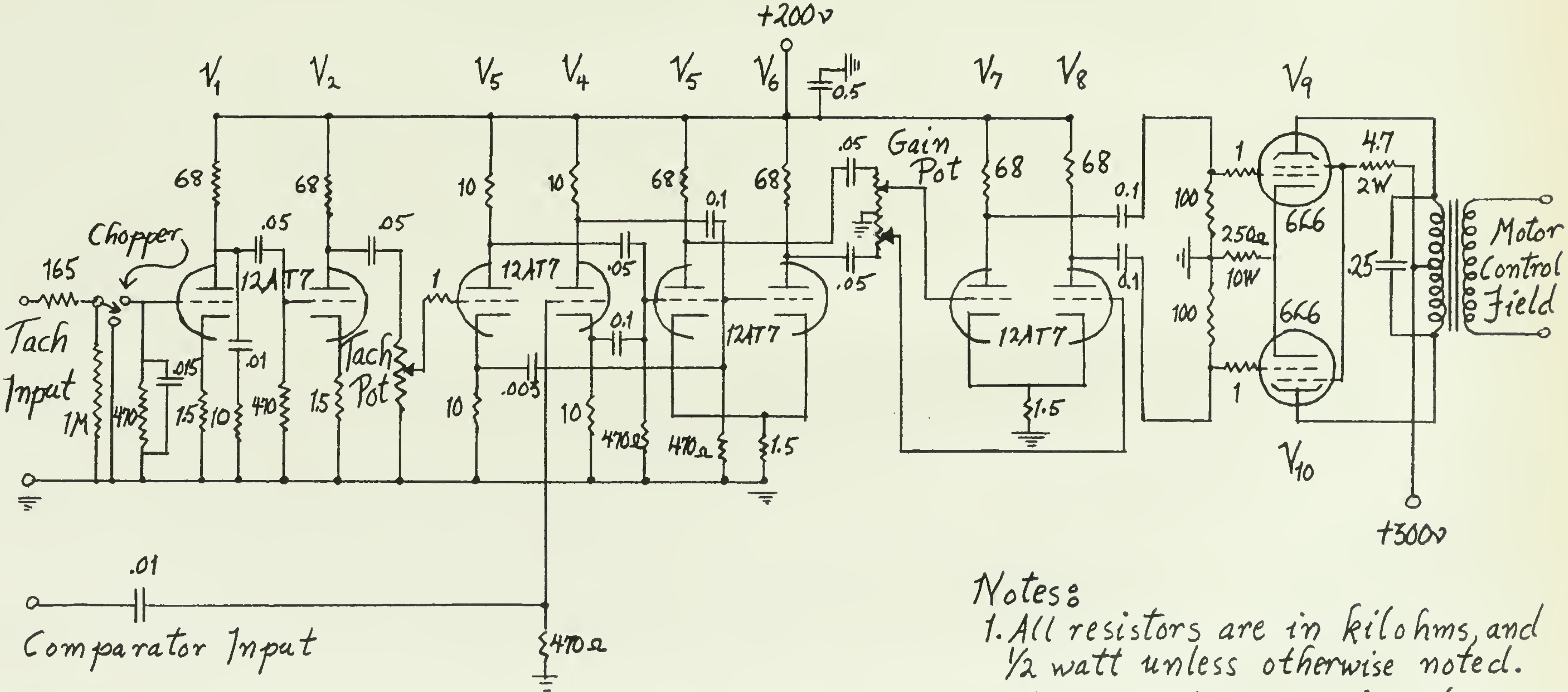


Notes:
1. All resistors are in kilohms, and ½ watt unless otherwise noted.
2. All capacitors are in $\mu f$.

Figure 5. Circuit Diagram of the 60 cps, A-C Servo Amplifier

2.6 Servo Motor and Tachometer

Figure 6 is a characteristic sheet for the Diehl FPE 25-86-1, 60 cps a-c, two phase Low Inertia Servo Motor with an integral d-c Tachometer which was used in the model servomechanism. Little need be said here about this component since it is a standard component.

Figure 7 is a detail picture showing how this motor-tachometer was mounted in conjunction with the PIC Design Corporation 1800:1 speed reducer and the Baldwin encoder.

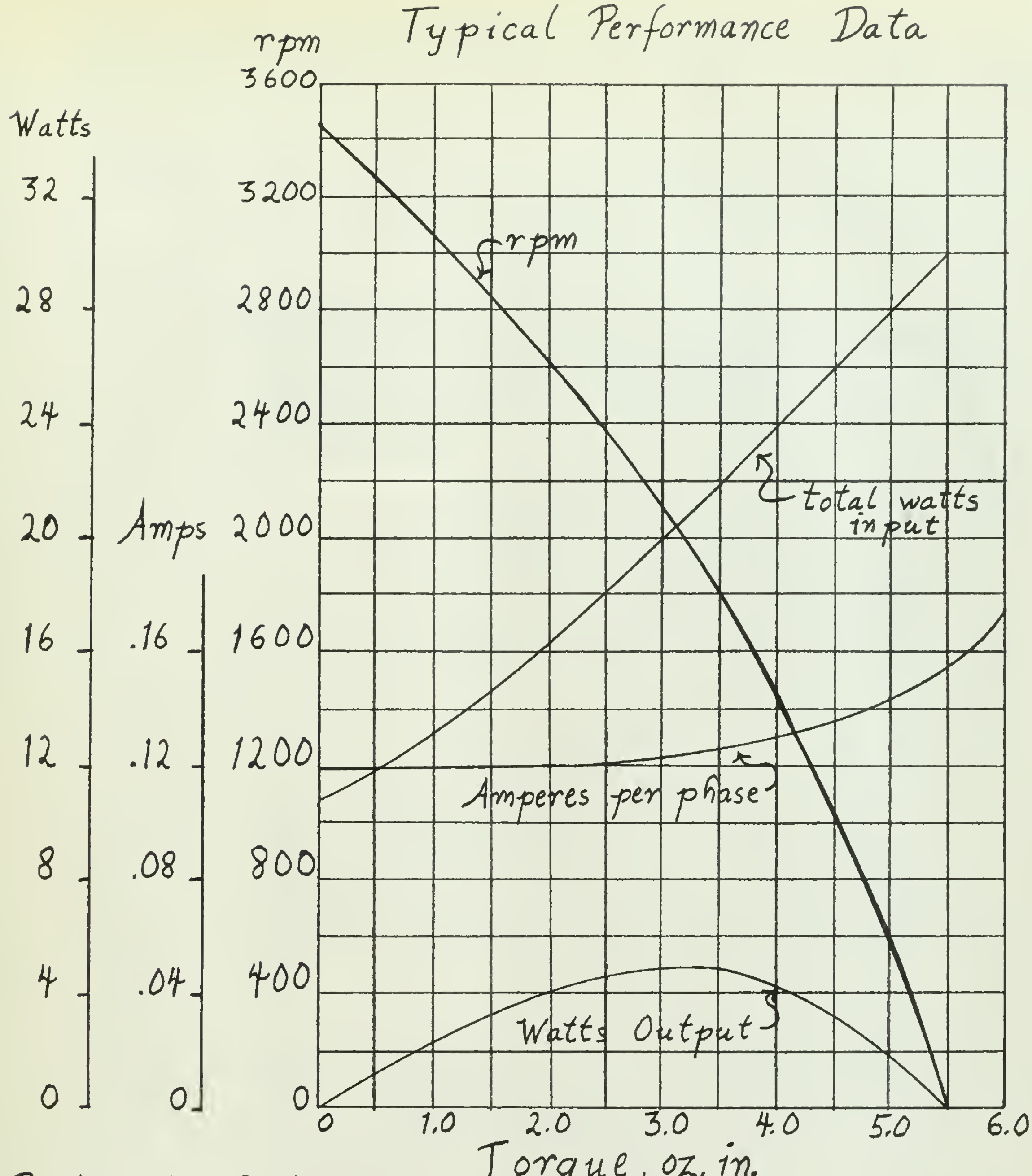


Pertinent Data:

115/115 v, 60 Cycle, 2 Phase, 2 pole, 3.5 Watt Output
Theoretical Acceleration @ Stall = 10,750 rad/sec$^2$
$Wk^2$ (Inertia) = 0.180 oz. in$^2$
D-C Tachometer Voltage = 6.5 volts per 1000 rpm

Note: All information shown given by Diehl Manufacturing Company

Figure 6. Characteristics of the Diehl FPE 25-86-1 A-C Low Inertia Servo Motor with Integral D-C Tachometer.

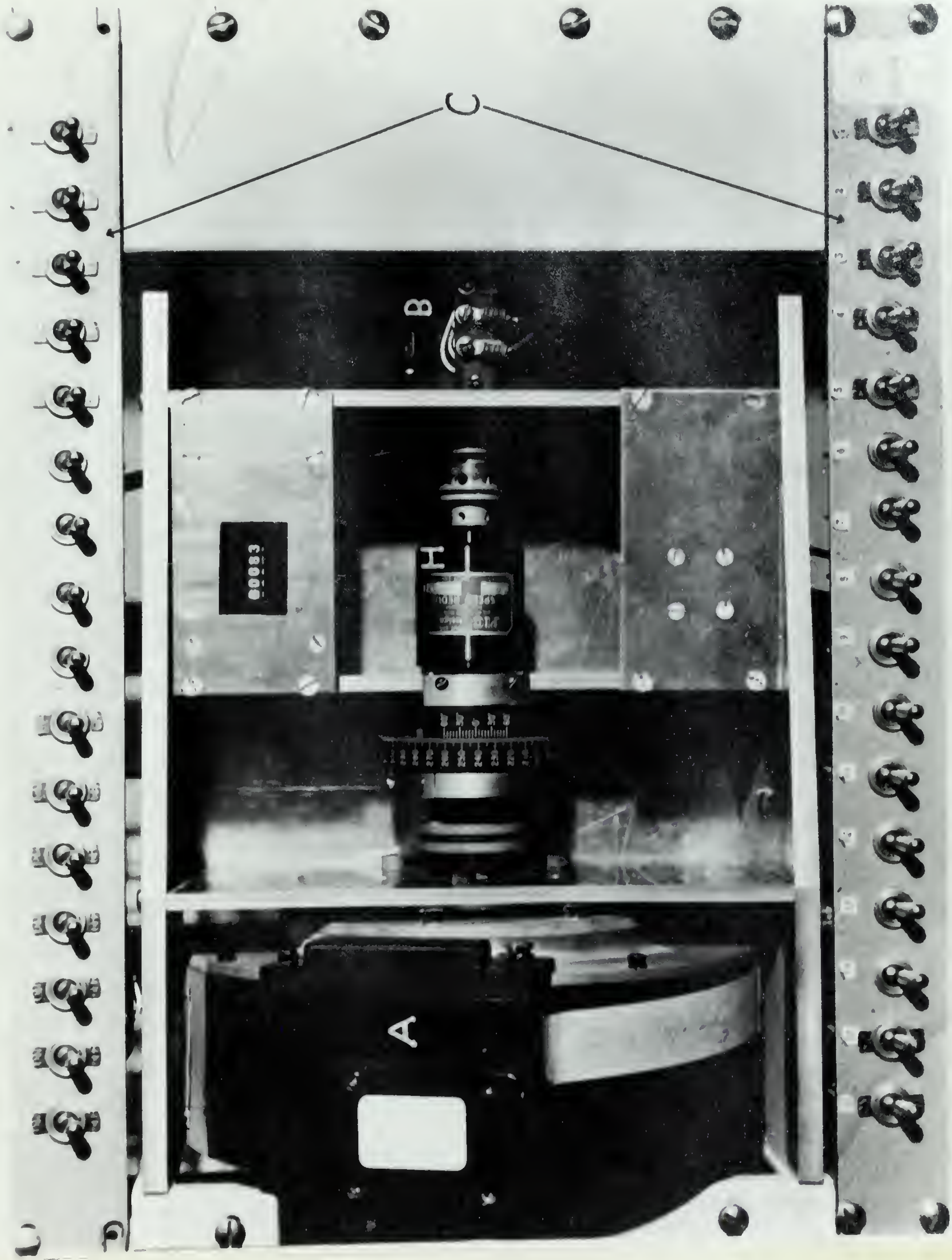


Figure 7. Experimental Servo Plant Consisting of Motor, Gear Train, and Shaft Encoder Load

# III TESTING PROCEDURES AND RESULTS

## 3.1 Testing Procedures

Since the Baldwin Encoder performs the function of a sampler in the system being studied, it was necessary to set the proper sampling rate of 25 samples per second. This was done by setting the pulsing rate of the encoder programmer which pulses the strobotron light in the encoder at 25 pulses per second.

It was required by the servo specifications that the static position error be no greater than one bit, that is, one part in 65,536. Therefore, the amplifier gain and rate feedback potentiometers were varied and step inputs were applied to the system by the upper switch panel of Figure 1. Each switch, representing a binary digit, sent a proper amplitude voltage to the input section of the comparator. The output position of the encoder shaft registered in true binary on the light panel of the translator, shown in Figure 1. For zero position error, the translator light configuration would exactly match the input register configuration. Runs were made until a proper setting of gain and rate feedback were obtained such that final position error was within one bit consistently for all inputs, from one bit up to large slew signals.

When a satisfactory gain and rate feedback setting was obtained a multi-channel Brush Recorder capable of speeds up to 250 mm per second was used to record (a) the comparator

output (error), (b) servo-amplifier output (control field voltage of the servomotor), and (c) tachometer d-c voltage. The latter was a measure of the motor speed through a manufacturer supplied correlation: 6.5 volts d-c per 1000 rpm. This correlation was checked by timing the revolutions of the encoder which was easily done because it ran much slower than the motor, and calculating the motor speed by multiplication of the gear ratio; the correlation was found to be accurate.

### 3.2 Results

The results obtained from tests are summarized below:

1. The servo system is velocity limited due to two limits:
   a. The comparator output is limited to .6 volts, rms.
   b. The amplifier saturates, putting out a maximum of 80 volts, rms for a .6 volt, rms input no matter how high the amplifier gain potentiometer is set.
2. In the light of the velocity limit, the maximum motor speed is obtained with no rate feedback, in which case its maximum speed is 355 radians/second, corresponding to $197 \times 10^{-3}$ radians/second for the system output shaft.
3. With no rate feedback, however, the system always goes into a limit cycle.
4. With rate feedback, only approximately one combination of amplifier gain and rate feedback gave satisfactory results of a minimum number of overshoots and no greater than one bit static error. Changing either more than slightly

resulted in either a limit cycle or a system whose gain was too low to respond to a one bit input signal.

5. It was found that at least 7 volts, rms control field voltage was required to drive the motor, which corresponded to a minimum amplification of 350, to respond to a one bit (.02 volt, rms) input signal.
6. Under static conditions if either the amplifier gain potentiometer or the rate feedback potentiometer were increased independently of the other a chatter or jitter developed. The rate feedback potentiometer was especially sensitive.
7. For the proper settings of gain and rate feedback resulting in a satisfactory response, the maximum motor speed (the velocity limit) was 137 radians/second, corresponding to $76 \times 10^{-3}$ radians/second for the system output shaft.
8. There is a large amount of backlash in the PIC 1800:1 Speed Reducer evidenced by long flat portions in the transients recorded by the Brush Recorder.
9. Finally, the Brush Recorder tapes show that the error never nulls out completely to zero, nor does the amplifier output, but for the satisfactory response case this electrical noise is not enough to cause the motor to jitter.

# IV DERIVATION OF TRANSFER FUNCTIONS OF COMPONENTS

## 4.1 Introduction

In this section, the transfer functions of the system components briefly described in Section II will be derived, making use of some of the observed data of Section III, for use in the mathematical analysis to follow.

## 4.2 Baldwin Encoder and Translator

As previously described, the function of the Baldwin optical shaft encoder is to convert the output shaft position to a 16 binary digit number on a separate track for each digit simultaneously (i.e. parallel conversion), reading out in Gray binary code. In the mechanics of this device the read-out is performed by photocells activated by a pulsing light passing through a coded disk attached to the shaft. It is this pulsing light which performs the function of a sampler which makes the system being studied a sampled data system. As previously mentioned, the sampling rate was specified as 25 samples per second in view of other aspects of the overall design.

The translator following the encoder has the basic function of translating the Gray binary shaft position to a true binary number, but it has a by-product function which is very important from a servo analysis standpoint. This second function is that each channel of the translator performs a zero order hold or clamping action on the digit in its channel between sampling instants.

Thus, the overall function of the encoder-translator combination is to sample and clamp the output shaft position and feed it back to the comparator to get a direct measure of position error, essentially a unity feedback function. The combination can be represented as in Figure 8.

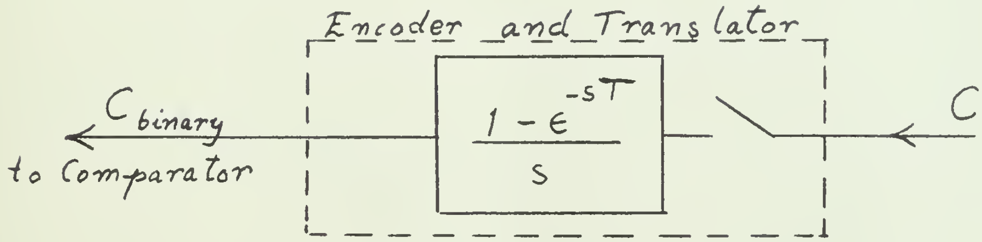


Figure 8. Block Diagram Representation of Shaft Encoder and Translator Combination.

### 4.3 Norden Ketay Digital Comparator

The basic function of the digital comparator is to form a voltage analog of the error signal by comparing two digital numbers, the input signal, and the translator output signal, and then transforming the difference into an a-c electrical voltage, the phase of which is determined by the sign of the difference. As mentioned in Section II, a true transformation of the difference is performed only when the difference is less than or equal to the binary number 32 ($2^5$). When the difference is greater than that, the a-c voltage output is a constant level. Due to the fact that the error is derived from a numerical difference the error signal produced is quantized, and each quanta, representing a binary one, has an rms value of approximately .018 volts. Figure 9 is the digital-to-voltage transformation characteristic of the comparator.

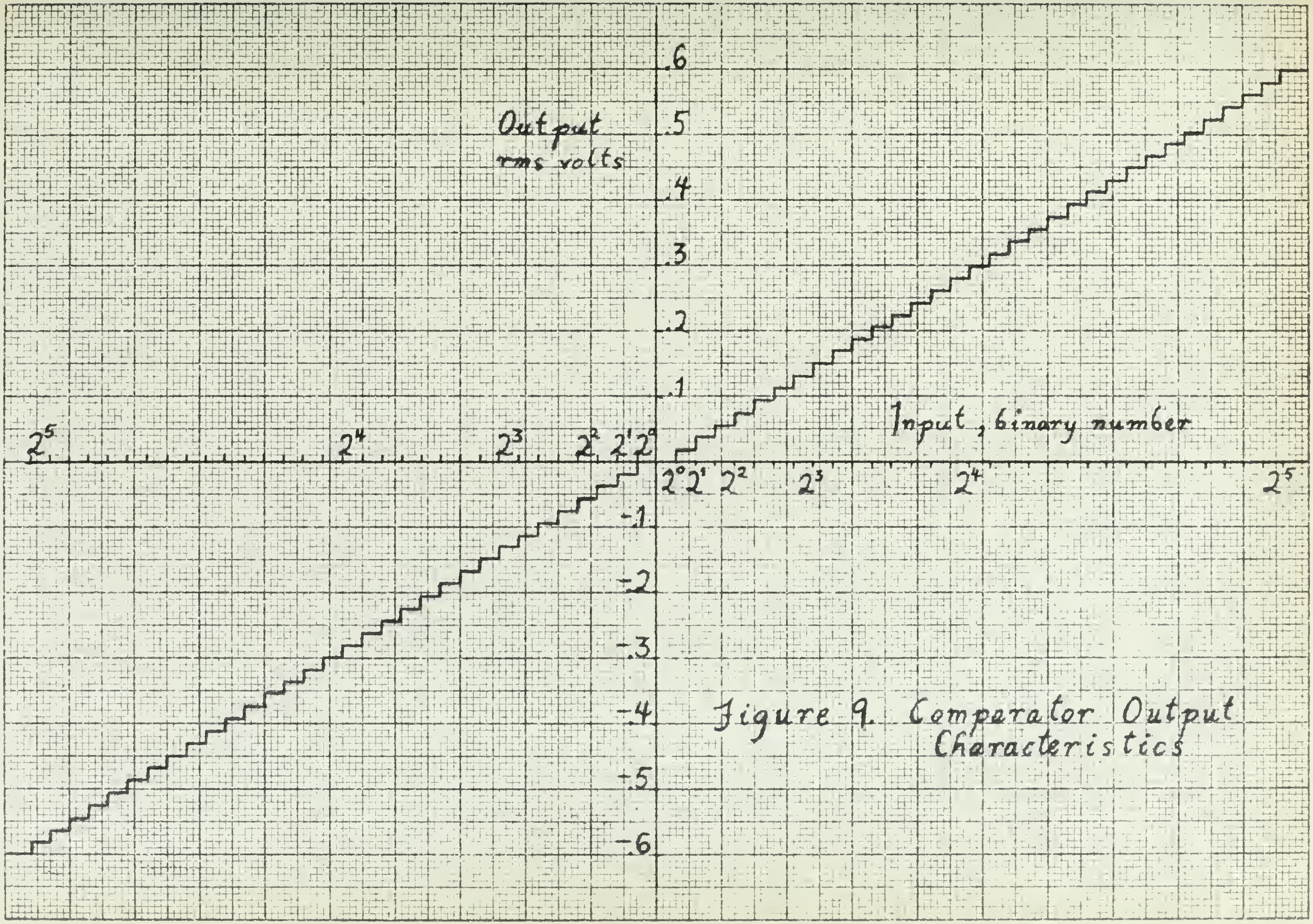


Figure 9. Comparator Output Characteristics

There is an additional scaling factor necessary to convert from binary numbers to radians, $K_e$, which is derived as follows:

$$\text{binary number 1, (1 "bit")} = \frac{2\pi}{2^{16}} = \frac{6.283}{65,536} = .968 \times 10^{-4} \text{ radians}$$

$$K_e = \frac{.018 \text{ volts}}{.968 \times 10^{-4} \text{ radians}} = 186 \text{ volts/radian}$$

The block diagram representation of the comparator is shown in Figure 10.

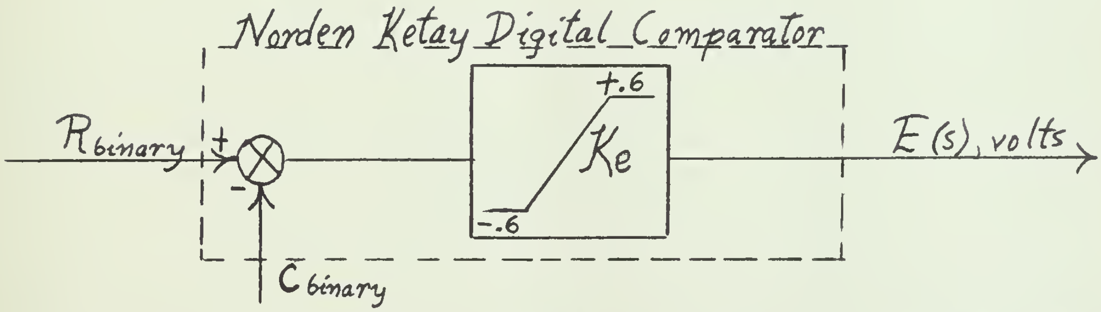


Figure 10. Block Diagram Representation of Norden Ketay Digital Comparator.

## 4.4 Servo Amplifier

Little need be said here as to the obvious function of the amplifier, but its saturation characteristics must be shown, so that its linear and nonlinear zones may be approximated for use in mathematical analysis.

As stated in Section III, it was determined that in the linear zone around zero error an amplification of at least 350 was required for the servo to respond to a one bit input signal, and it was also found that even with rate feedback for stabilization the amplifier gain could not be set too much higher than this. Therefore, the amplifier gain characteristic was determined for this setting and is shown in Figure 11. As can be

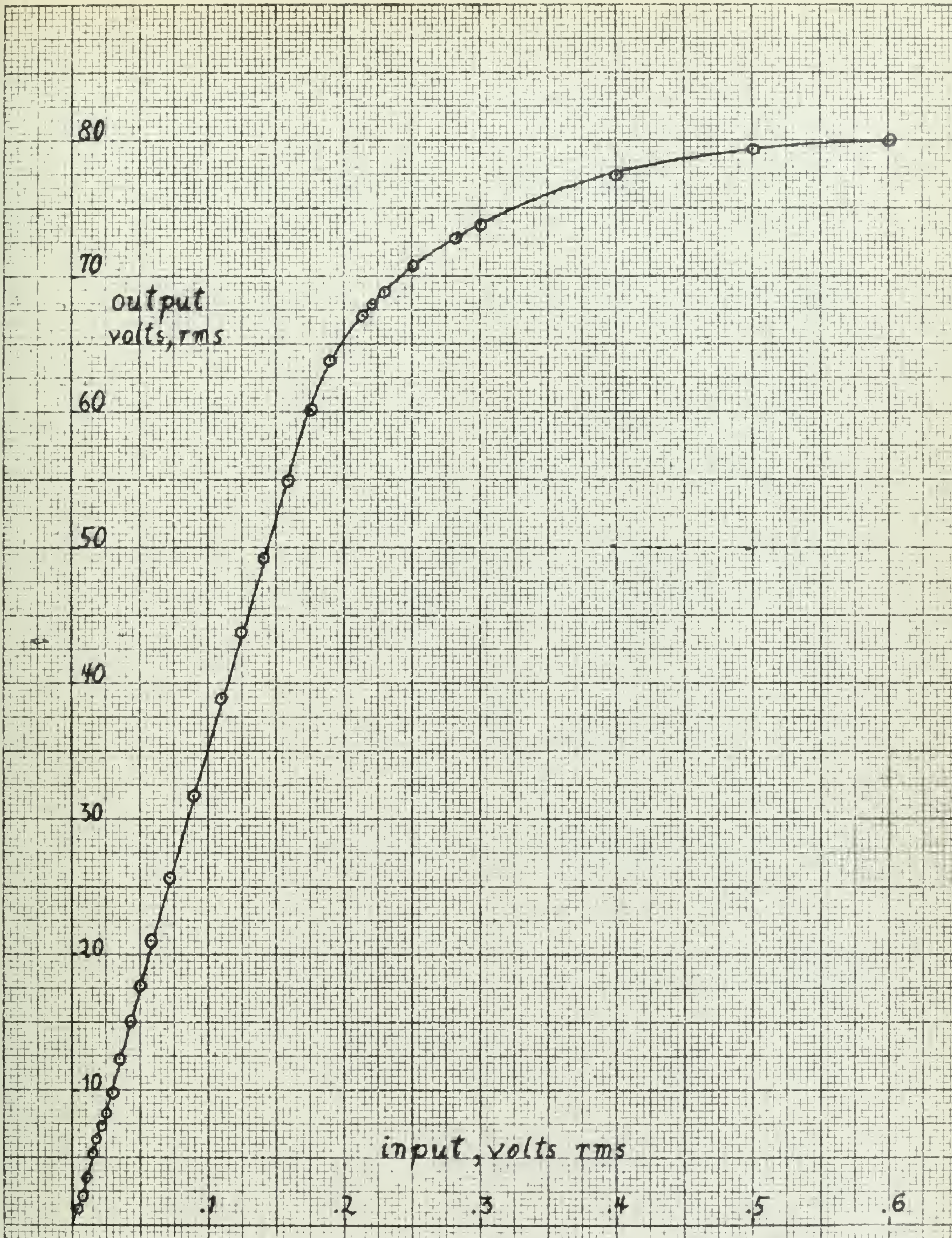


Figure 11. A Typical Servo Amplifier Saturation Characteristic.

seen, the amplifier transfer function can be divided into three zones:

(1) for input less than .2 volts, rms:

$$K_a = 350$$

(2) for input equal to or greater than .6 volts, rms:

$$K_a = 80/.6 = 133.3$$

(3) for inputs between .2 and .6 volts, rms there is a transition zone where $K_a$ is changing between the above limits.

For some parts of the mathematical analysis the transition zone will be neglected, and the amplifier can be represented as in Figure 12.

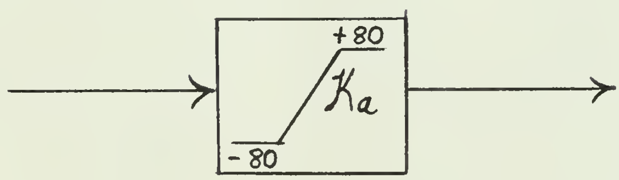


Figure 12. Block Diagram Representation of Servo Amplifier.

4.5 Diehl Servomotor and Tachometer

In accordance with reference (3), a two-phase servomotor transfer function can be approximated as:

$$KG = \frac{K_m}{s(s\tau_m + 1)}$$

where:

$$K_m = \left|\frac{\partial \omega}{\partial V_c}\right|$$

$$\tau_m = \frac{J}{\left|\frac{\partial T}{\partial \omega}\right|} \times (2.59 \times 10^{-3})$$

$\omega$ = speed, rads./sec

$V_c$ = motor control field voltage

$J$ = polar moment of inertia, oz-in$^2$

$T$ = torque, oz-in

Although in Figure 6 the torque versus speed curve is shown only for rated reference and control field voltage, the common assumptions were made that torque versus speed curves for other values of $V_c$ are approximately parallel to the one given, and that the slope of these curves can be approximated linearly so that torque versus speed can be assumed a constant. Thus, from Figure 6:

$$\left|\frac{\partial T}{\partial \omega}\right| \doteq \frac{5.5 \text{ oz-in}}{3450 \text{ rpm}} = \frac{5.5 \text{ oz-in}}{3450(2\pi)/60 \text{ rads/sec}}$$

Since this motor has to operate over full speed range, this broad, end point slope was considered the best approximation.

Two phase servomotors are designed to have a linear relation between stall torque and control field voltage, and this was determined to be approximately true as shown in Figure 13. From this figure it is determined that:

$$\left|\frac{\partial T}{\partial V_c}\right| \doteq \frac{3.2 \text{ oz-in}}{68 \text{ volts}}$$

Therefore:

$$K_m = \left|\frac{\partial \omega}{\partial V_c}\right| = \frac{\left|\frac{\partial T}{\partial V_c}\right|}{\left|\frac{\partial T}{\partial \omega}\right|} \doteq \frac{\frac{3.2}{68}}{\frac{5.5}{3450(2\pi)/60}} = 3.08 \ \frac{\text{rad/sec}}{\text{volt}}$$

For the determination of the time constant, $\tau_m$, the moment of inertia, J, consists of motor and connected tachometer inertia, $J_m$, given in Figure 6, plus the load inertia transferred through the gear train. It was found that the inertia of the Baldwin Encoder (the load) is 18.2 lb.-in$^2$.

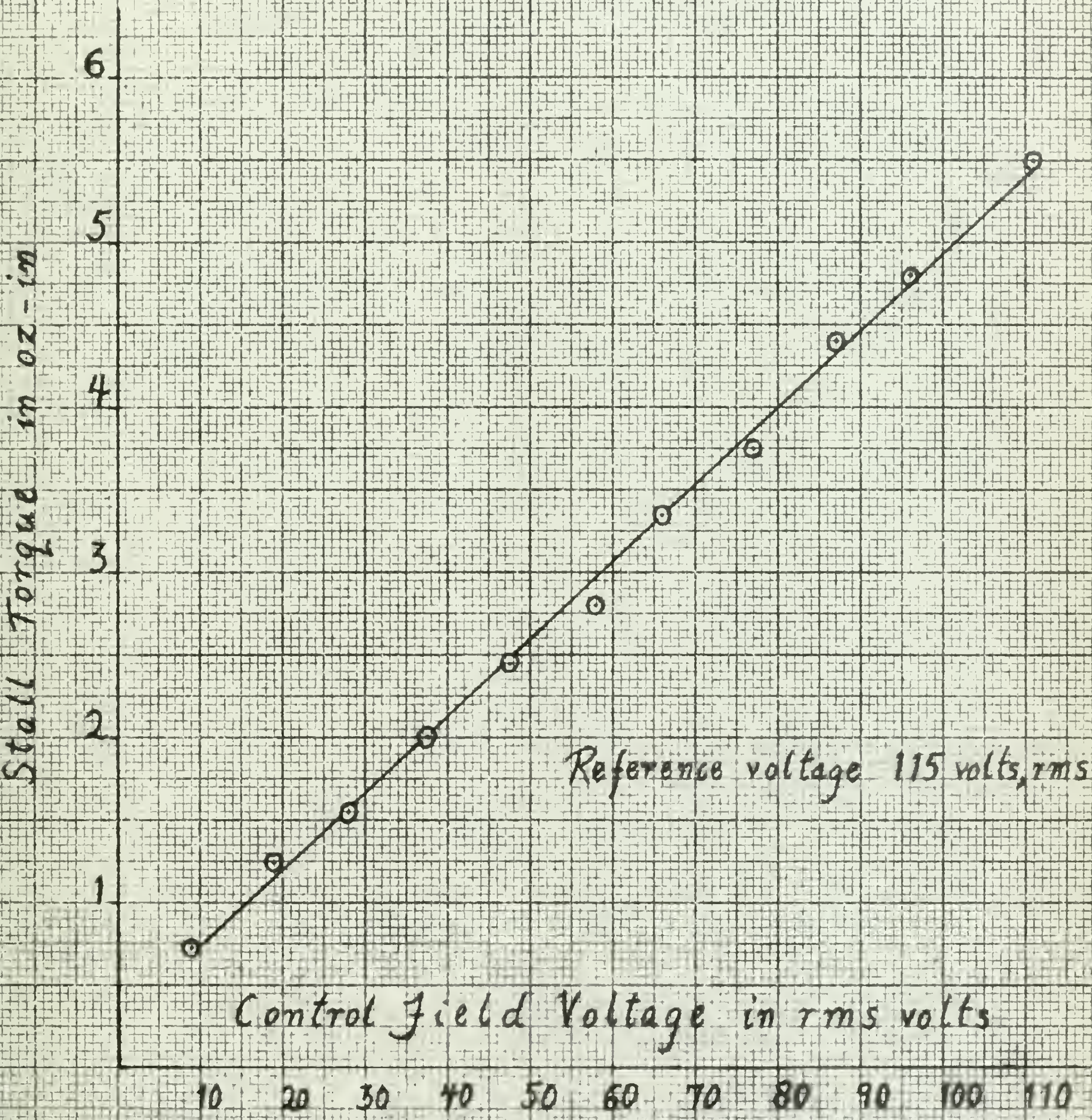


Figure 13. Stall Torque Characteristics of the Diehl FPE 25-86-1 Two Phase, 60 cps Servo motor.

Transferring back through the gear train this becomes:

$$\rho^2 J_L = \frac{1}{(1800)^2}\left[(18.2)(16)\right] \text{ oz-in}^2$$

As can be seen, because of the large gear ratio, the load contribution to J is small compared to $J_m$, so it was neglected. Therefore:

$$\tau_m = \frac{J}{\left|\frac{\partial T}{\partial \omega}\right|} \times (2.59 \times 10^{-3}) = \frac{.18}{\frac{5.5}{3450(2\pi)/60}} \times (2.59 \times 10^{-3}) = .0306 \text{ sec.}$$

The tachometer transfer function is simply a scale factor, $K_T$ , times s . The motor-tachometer block diagram is shown in Figure 14.

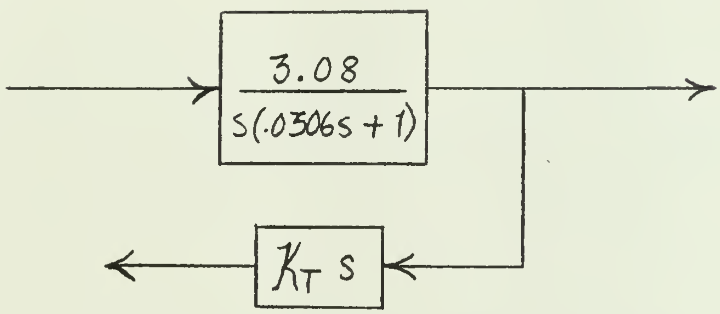


Figure 14. Block Diagram Representation of Motor and Tachometer.

## 4.6 The Overall System

Summarizing and putting together the block diagrams of all the component parts, an overall system block diagram is arrived at. This system block diagram is shown in Figure 15 on the following page.

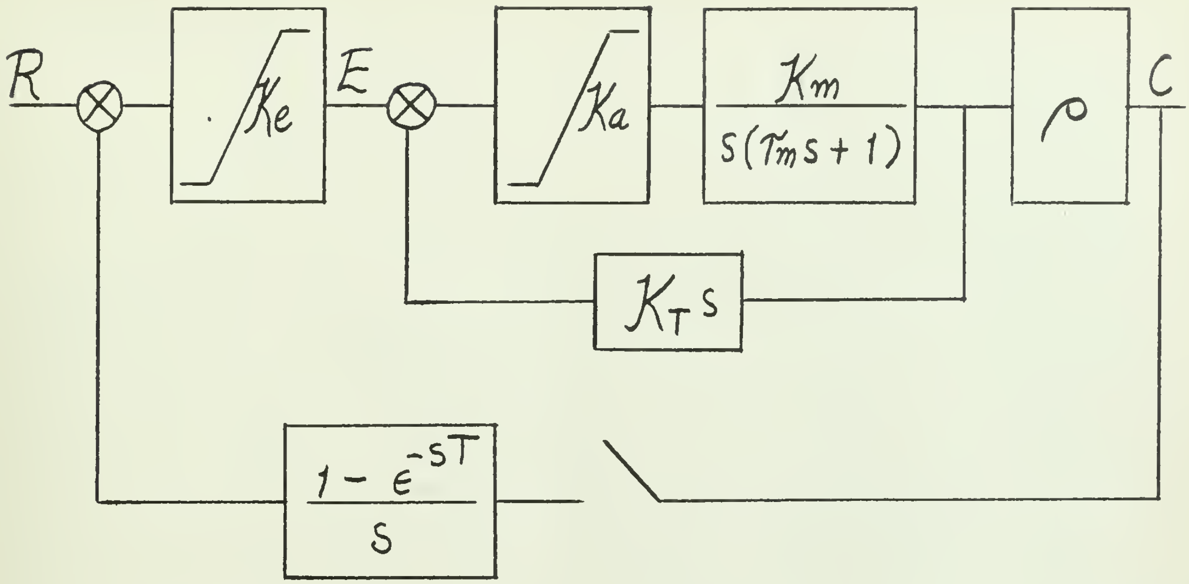


**Figure 15.** Block Diagram Representation of the Entire Servo System.

In Figure 15 symbols have been used rather than numerical values for convenience in analysis. For the sake of simplicity in analysis the inner loop can be reduced to a single block, and thus the system reduces to that of Figure 16.

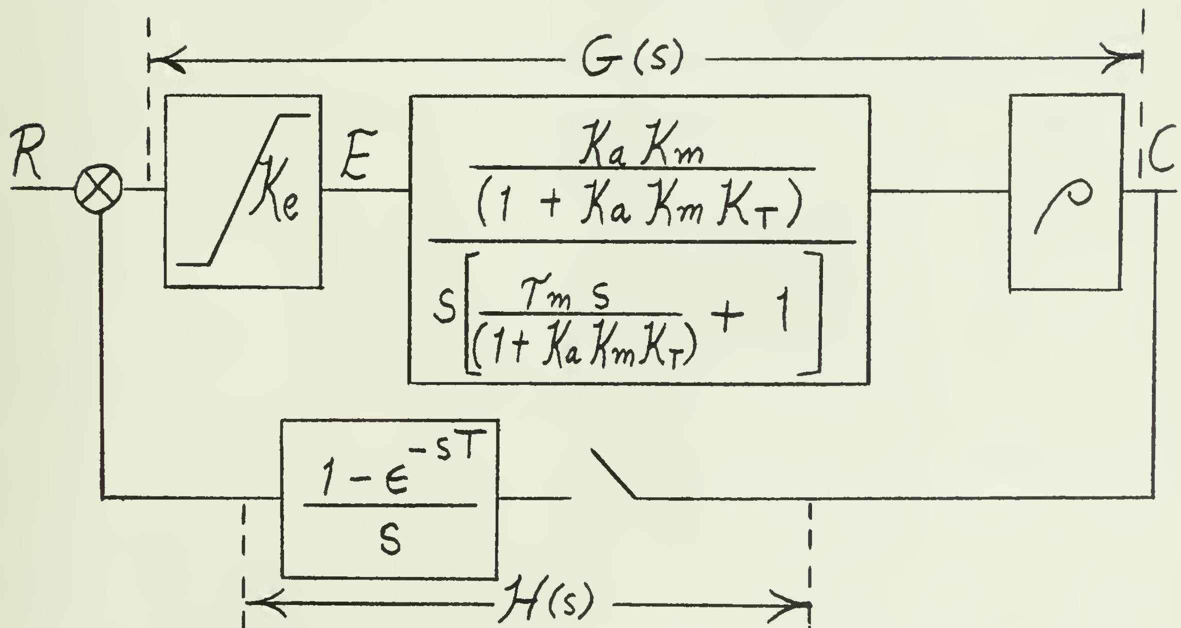


Figure 16. Single Loop Block Diagram of the System.

## V MATHEMATICAL ANALYSIS OF SYSTEM AND COMPARISON WITH OBSERVED DATA

### 5.1 Introduction

In this section the mathematical analysis of the model servomechanism will be presented and a comparison will be made between the theoretical and observed results given in Section III with a discussion as to the reasons for differences. The basic analytical tools to be used in this analysis are the root locus of sampled data systems, the principles of which are found in references (4) and (5), and a graphic method for obtaining the transient response to a step input for a sampled data system which contains a zero order hold following the sampler developed in reference (5).

### 5.2 Root Locus Analysis for System Without Rate Feedback

As the observed data of Section III shows, the system is velocity limited and further, the greatest limiting velocity is obtained with zero rate feedback. However, observation also showed that there is always a limit cycle in this case. Since the system being considered is second order, the reason for this instability is not immediately evident, but a root locus analysis in conjunction with another bit of observed data will reveal the reason.

Referring to Figure 16, when $K_T = 0$, in the linear operation zone (E less than .2 volts, rms), the direct transfer function, G(s), reduces to:

$$G(s) = \frac{K_e K_a K_m/\rho}{s(\tau_m s + 1)} = K_e K_a K_m/\rho \left\{ \frac{1/\tau_m}{s(s + 1/\tau_m)} \right\}$$

Putting in numerical values derived in Section IV:

$$G(s) = (186)(350)(3.08)/1800 \left\{ \frac{1/.0306}{s(s+1/.0306)} \right\} = 111 \left\{ \frac{32.7}{s(s+32.7)} \right\}$$

The characteristic equation, as a sampled data system is:

$$1 + 111 \mathcal{Z} \left[ \left\{ \frac{32.7}{s(s+32.7)} \right\} \left\{ \frac{1-\epsilon^{-sT}}{s} \right\} \right] = 0$$

where Z means " the z transform of ". Taking the z transform, after first expanding by partial fractions, the result is, going back to symbols instead of numerical values again for the moment:

$$GH(z) = K_e K_a K_m \rho \left\{ \frac{\left[ T/\tau_m - (1-\epsilon^{-T/\tau_m}) \right] \left[ z + \dfrac{\left\{ (1-\epsilon^{-T/\tau_m}) - T/\tau_m \, \epsilon^{-T/\tau_m} \right\}}{\left\{ T/\tau_m - (1-\epsilon^{-T/\tau_m}) \right\}} \right]}{\frac{1}{\tau_m} (z-1)(z-\epsilon^{-T/\tau_m})} \right\}$$

Recalling that the sampling rate was specified as 25 samples per second, then the sampling period, T =.04 secs. Using this and other known numerics, leaving amplifier gain, however, as a symbol, the above expression reduces to:

$$GH(z) = \frac{.00563 K_a (z+.649)}{(z-1)(z-.27)}$$

The root locus of GH(z) is shown in Figure 17. The stability limit is where the root locus crosses the unity circle on the z-plane, and this occurs for an overall gain constant, consisting in this case of $.00563K_a$, of 1.11. Thus,

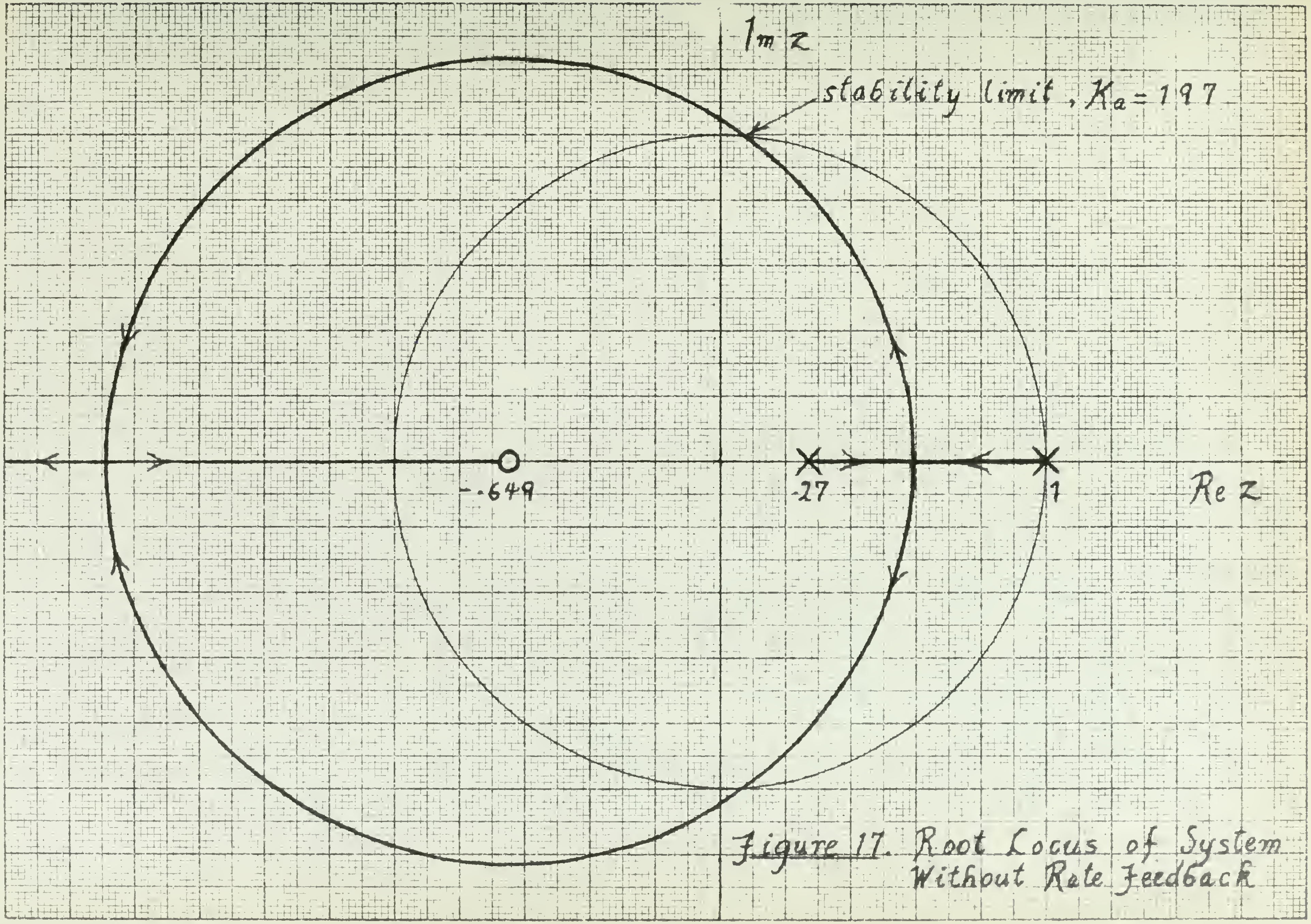


Figure 17. Root Locus of System Without Rate Feedback

it is found that for stability, $K_a$ has an upper bound of:

$$K_a(max) = \frac{1.11}{.00563} = 197$$

Since it was found necessary in the actual system to have $K_a$ at least 350 to respond to a one bit signal, as indicated in Section III, it is evident that rate feedback, or other compensation, must be used. Because of its simplicity, rate feedback was used.

5.3 Root Locus Analysis of Rate Feedback Damped System

Before proceeding with the analysis, it is necessary to show how the rate feedback constant, $K_T$, is determined as a numerical value. Referring again to Figure 16, the velocity constant of the plant is:

$$\text{Plant Velocity Constant} = \frac{K_a K_m}{1 + K_a K_m K_T} \quad \frac{\text{rads/sec}}{\text{volt}}$$

For step inputs this velocity constant relates the output speed of the motor (not the output speed of the system) to the input error signal as a voltage. As mentioned in Section III, for the satisfactorily damped case, while the comparator was saturated, a multi-channel Brush Recorder recorded pertinent quantities, and the output shaft speed was measured. Thus, from observed data motor limit velocity and error voltage are known quantities, and for this condition the amplifier was in full saturation, so $K_a = 133.3$, and $K_m$ is known. Therefore, for this condition $K_T$ can be determined.

However, the question arises, what happens when the

comparator comes out of saturation and $K_a$ gradually increases from 133.3 to 350? To answer this question corresponding points in time as the servo came into correspondence were taken, and the results are shown in Table I below.

Table I. Observed Plant Parameters for Satisfactorily Damped Rate Feedback System.

| E volts, rms | Motor Velocity rads/sec | $K_a$ | $K_T$ | $K_a K_m K_T$ | Plant Velocity Constant | Plant Time Constant |
|---|---|---|---|---|---|---|
| .6 | 137 | 133.3 | .00195 | .8 | 228 | .017 |
| .5 | 133.3 | 156 | .00167 | .8 | 267 | .017 |
| .2 | 105 | 325 | .008 | .8 | 525 | .017 |

Table I shows, then, that the product $K_a K_m K_T$ remains a constant, and that the plant time constant is changed, and the Plant Velocity Constant is reduced by the rate feedback, which are well-known facts.

Therefore, for the satisfactory rate damped system, referring again to Figure 16, in the linear operation zone (E less than .2 volts, rms):

$$G(s) = \frac{K_e K_a K_m \rho / (1 + K_a K_m K_T)}{s\left[\frac{\tau_m s}{(1 + K_a K_m K_T)} + 1\right]} = \frac{K_e K_a K_m \rho}{(1 + K_a K_m K_T)} \left\{ \frac{(K_a K_m K_T + 1)/\tau_m}{s\left[s + (K_a K_m K_T + 1)/\tau_m\right]} \right\}$$

Putting in numerical values, this becomes:

$$G(s) = 61.9 \left\{ \frac{58.8}{s(s + 58.8)} \right\}$$

Since this has the same form as the undamped G(s) of paragraph 5.2, the plant as a function of z has the same form, and results in:

$$GH(z) = 1.52\left\{\frac{(z+.471)}{(z-1)(z-.0952)}\right\}$$

The root locus of GH(z) is shown in Figure 18, and the operating point for the above gain constant, is shown. Also shown is the operating point during full saturation when $K_a = 133.3$, and the z-plane gain constant is reduced from 1.52 to .58. Thus is shown the fact that saturation can be regarded as a reduction in effective gain as stated by reference (6) and other authors.

An observed fact was that the amplifier gain could not be increased appreciably without causing a limit cycle even with rate feedback. The reason is clearly evident in Figure 18, since in the linear zone, with $K_a = 350$, the operating point is very close to the unity circle.

5.4 Transient Analysis of Rate Feedback Damped System

In calculating the transient response of this sampled data system for comparison with the observed transient, the method to be used is graphic build-up of the transient response. The method is suggested in reference (5) and it takes advantage of the fact that, due to the zero-order hold properties of the **translator** following the encoder, the error signal can be considered composed of step functions delayed in time by multiples of the sampling period, and thus the transient

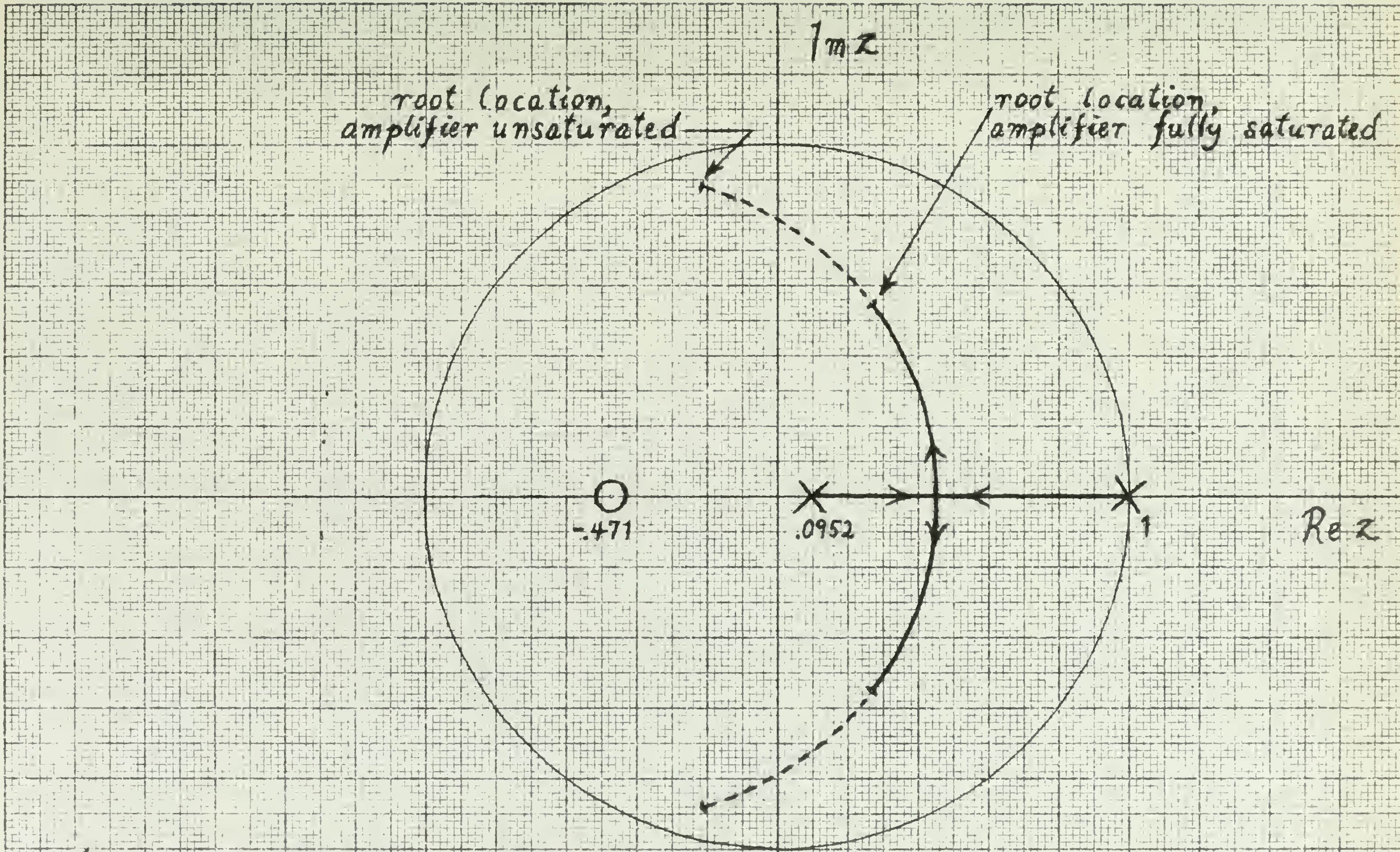


Figure 18. Root Locus of Rate Feedback Damped System.

response can be readily computed using step function response and the superposition principle.

For the system under consideration, using the numerical values for G(s) of Figure 16 calculated in subsection 5.3:

$$C(s) = G(s)E(s) = 61.9\left\{\frac{58.8}{s(s+58.8)}\right\} E(s)$$

E(s) at each sampling instant can be considered a delayed step function, the amplitude of which is the difference between the true error at this time and the true error at the previous sampling instant, thus:

$$C(s) = 61.9\left\{\frac{58.8}{s(s+58.8)}\right\}\left[\frac{A_0}{s} + \frac{(A_1 - A_0)\epsilon^{-Ts}}{s} + \cdots + \frac{(A_n - A_{n-1})\epsilon^{-nTs}}{s}\right]$$

Taking the inverse Laplace Transform, the time solution is:

$$C(t) = 61.9\left(t - \frac{1}{58.8} + \frac{1}{58.8}\epsilon^{-58.8t}\right)\left[A_0 u(t) + \cdots + (A_n - A_{n-1})u(t - nT)\right]$$

From the above the transient solution is graphically built up, using the relation below to determine the amplitudes of the delayed steps:

$$A_n - A_{n-1} = |E|_{t=nT} - |E|_{t=(n-1)T} = R - C(t)_{t=nT} - \left[R - C(t)_{t=(n-1)T}\right]$$

$$= -C(t)_{t=nT} + C(t)_{t=(n-1)T}$$

From the above equations the transient response for the linear zone, that is for $K_a = 350$, for an input step of $3.22 \times 10^{-3}$ radians (.6 volts, rms as a voltage) was determined

and is shown in Figure 19. Note that it is unnecessary to consider larger step inputs here due to comparator saturation.

However, this does not tell the whole story, because $K_a$ varies throughout the region depending upon the instantaneous value of E. Therefore, a second transient solution was calculated for the full amplifier saturation zone where $K_a = 133.3$. The only difference in the time solution equation is the constant multiplier which is 23.6 in the full amplifier saturation case instead of 61.9. This transient is also shown in Figure 19.

The true transient taken from Brush Recorder tape is shown for comparison on Figure 19, and as one would expect, it appears to fall somewhere between the fully saturated and unsaturated amplifier transients. Quite notable also is the long flat portion which is the effect of the very large gear train backlash.

### 5.5 Discussion of Analysis and Observed Results

For the most part, the mathematical analysis presented agrees reasonably well with the observed results of Section III. The most pronounced nonlinear effects observed, insofar as they effect the performance of the servomechanism, are the saturation, or limiting effects of the comparator and the servo amplifier. These saturation effects were taken into consideration in the mathematical analysis and for that reason the analysis gives reasonable explanations for the observed effects. In particular, the root locus analysis for the undamped system (subsection 5.2) shows that the limit cycle

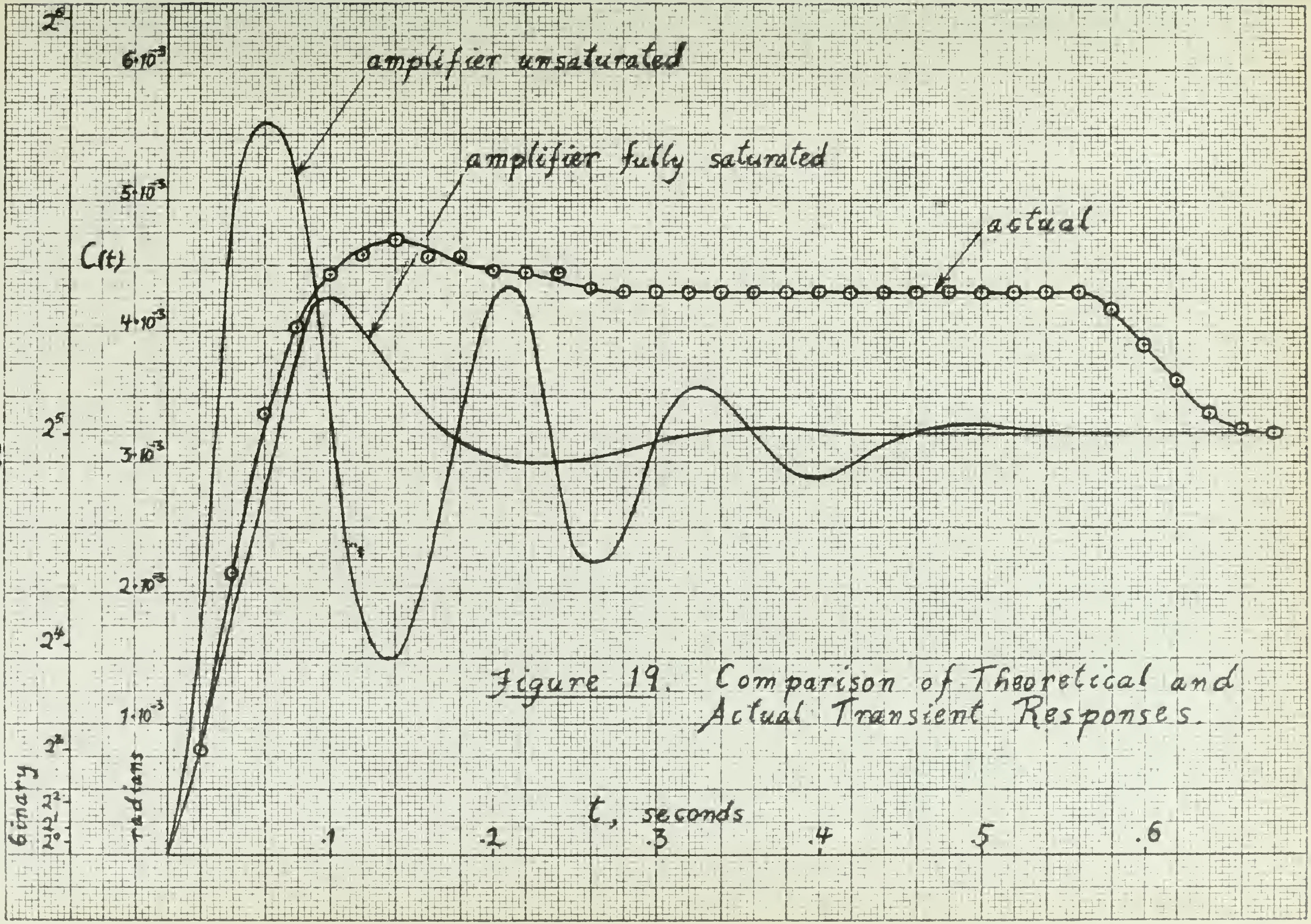


Figure 19. Comparison of Theoretical and Actual Transient Responses.

was caused by an amplifier gain which put the operating point outside the unity circle on the z-plane. This too high amplifier gain was observed necessary, however, for the system to respond to a one bit signal, and therefore, rate feedback or other compensation was a necessity.

The root locus analysis of the rate feedback damped case, (subsection 5.3), sheds light on the reason a very limited tolerance was permissible on the amplifier gain and rate feedback proportion. In the first place, the analysis shows that $K_a$ and $K_T$ are not independent, but directly affect both the plant time constant and the effective plant velocity constant. The root locus, Figure 18, shows clearly that $K_a$ for the linear zone could not be increased very much without putting the operating point on or outside the unity circle. It is true, theoretically, that the rate feedback could be increased to produce more damping, but actually this would probably make the system too sluggish to respond to a one bit signal. It must be recalled also that the rate feedback control was particularly sensitive to causing static chatter if set very high (see subsection 3.2, 9).

In the transient analysis, (subsection 5.4), boundary transient responses at the limits of amplifier values, (fully saturated, and unsaturated), show the extreme cases, and as Figure 19 shows, the actual transient falls between them as is to be expected. Comparing, the rise times on Figure 19, it is evident that the true transient most closely follows the full amplifier saturation curve in this region, which is

reasonable.

Aside from the saturation effects, the most noticeable observed nonlinearity was the large backlash, shown quite clearly in Figure 19. However, the mathematical analysis, although not taking it into consideration, has given reasonable explanations for limit cycles observed. Since limit cycles are the most pronounced effect of large backlash, it seems that backlash does not affect the system performance in this way; this is borne out by the transient where, although there is a large flat portion due to backlash, there is no limit cycle.

Chestnut and Mayer, in reference (6), conclude that backlash tendency to produce limit cycles can be greatly reduced or eliminated by having as much of the total inertia as possible located in the load, which is certainly the case here where:

$$\frac{J_m}{J_L} = \frac{0.18 \text{ oz-in}^2}{(18.2)(16) \text{ oz-in}^2}$$

The transient of Figure 19 exhibits another interesting peculiarity. Note that there is a slight hump before the effect of backlash takes hold; this does not generally occur in continuous systems. It is the author's opinion that the answer lies in the sampling and zero order hold data reconstruction with its quantization and inherent time delay. Because of this the motor is not being controlled by the true instantaneous error of the system which is continuous, but by

approximation composed of discrete steps. Thus, the motor does not come to a smooth stop and then reverse direction as in a continuous system. If this were the case there would be no hump but just a constant error while the motor is taking up the backlash. Instead, the motor reversal tends to be jerky, as a function of the quantization, allowing the hump shown to occur.

Again, looking at Figure 19, it appears that the large amount of backlash tends to smooth out the response, since there is only a one-sided overshoot. By the time the motor has taken up the backlash, it is running at a constant, relatively slow speed, corresponding to an error of only about $1 \times 10^{-3}$ radians, and then merely drives into correspondence without additional overshoot.

All the other observed effects of subsection 3.2 are jitter effects. R. L. Hovious, in reference (7) has studied several of the contributing factors in a 60 cycle a-c servo, which is the type of servo being studied here. Among the most notable jitter causing factors are granularity and quantizing, particularly effective in a digital system such as this one, amplifier pick-up, at high gain especially, vibrator noise in chopper amplifiers, especially at high gain (this latter probably accounts for the rate feedback potentiometer being especially sensitive to causing jitter), and d-c unbalance between halves of the push-pull output stage of the amplifier.

# VI DUAL MODING FOR FAST RESPONSE TO LARGE STEP INPUTS

## 6.1 Introduction

In this section the problem of improving the time of response of the servomechanism for large step inputs which saturate the system is studied.

It was shown in the last section that rate feedback may be used to obtain a stable system. However, it is the very nature of rate feedback to decrease the velocity constant of the system, and thus, because the system is velocity limited, the maximum velocity attained is lower than that attained without rate feedback. Therefore it will inherently take longer for the system to reach correspondence when the input is a large step. By virtue of the fact that the system under study goes into full saturation for all inputs greater than $3.22 \times 10^{-3}$ radians, this is a serious disadvantage.

It is the opinion of the author that the simplest and most logical approach to overcoming this disadvantage is dual-moding.[1] A method was found whereby the servo is made to run with zero rate feedback, and thus maximum possible speed, whenever the true error is very much greater than $3.22 \times 10^{-3}$ radians. When the true error is reduced to approximately fifty per cent greater than $3.22 \times 10^{-3}$ radians,

[1]It would have been possible to try acceleration feedback which might have stabilized the system and still allow the motor to run at top speed, but it is felt that, in this particular case, dual-moding offers a simpler approach from an implementation viewpoint, as will be clear later.

rate feedback is switched in and the system drives into correspondence.

## 6.2 Phase Plane Analysis of a Continuous Data Approximation of the Rate Feedback Damped System

When one speaks of a dual mode servomechanism, he refers to a servomechanism, the performance of which cannot be described by a single differential equation throughout its range of operation. Instead, its performance can be roughly broken up into two regions, with a differential equation applicable to each region. These regions are so chosen that within them the system performance can be described by a linear differential equation. For this reason, such a system is often called a piece-wise linear system.

The simplest method of analyzing dual mode operation for a second-order servo is on the phase plane. However, phase plane methods are directly applicable only for continuous data systems. On the other hand, to date very little has been accomplished in working out analytic methods for handling nonlinear sampled data systems, and therefore the author has chosen to approximate the system under study by a continuous data system and to compare the phase trajectory obtained with an actual system trajectory from observed data.

In Figure 20 is shown a block diagram of a continuous data system with the same plant as the rate feedback damped system of subsections 5.3 and 5.4.

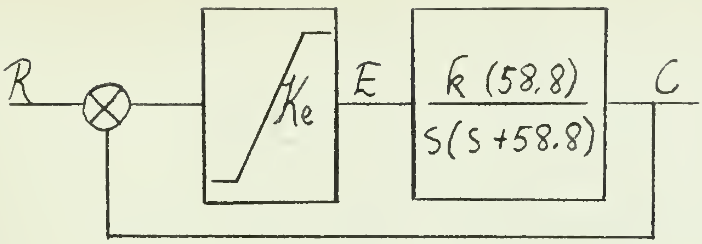


$$\text{where } k = \frac{\rho K_a K_m}{1 + K_a K_m K_T} = \frac{\rho K_a K_m}{1.8}$$

Figure 20. Continuous Data Approximation of the Stable Rate Feedback Damped System

From Figure 20:

$$\frac{C}{R} = \frac{\dfrac{K_e k\,(58.8)}{s(s+58.8)}}{1 + \dfrac{K_e k\,(58.8)}{s(s+58.8)}} = \frac{K_e k\,(58.8)}{s^2 + 58.8s + K_e k\,(58.8)},$$

$$C\,[s^2 + 58.8s + K_e k(58.8)] = K_e k\,(58.8)R,$$

$$(R - E)[s^2 + 58.8s + K_e k(58.8)] = K_e k\,(58.8)R,$$

$$Rs^2 + 58.8Rs \cancel{+ K_e k(58.8)R} - [Es^2 + 58.8Es + K_e k(58.8)E] = \cancel{K_e k\,(58.8)R}$$

Considering the Laplace variable as a differential operator:

$$\ddot{R} + 58.8\dot{R} = \ddot{E} + 58.8\dot{E} + K_e k\,(58.8)E$$

When R, the Input, is a step function:

$$\ddot{E} + 58.8\dot{E} + K_e k\,(58.8)E = 0$$

Now, manipulating into the proper form for use of the isocline method (8):

$$\frac{\ddot{E}}{\dot{E}} = N = -58.8 - K_e k\,(58.8)\frac{E}{\dot{E}}$$

$$\frac{\dot{E}}{E} = -\frac{K_e k\,(58.8)}{N + 58.8}$$

The last equation is the general isocline equation for

the system. The constant in the numerator has different values, depending upon the magnitude of $K_a$, which, in turn, is dependent upon the magnitude of the error. Considering the amplifier saturation characteristics, as in subsection 4.4:

(1) When the error is less than $1.075 \times 10^{-3}$ radians (.2 volts, rms), $K_a = 350$, and:

$$\frac{\dot{E}}{E} = \frac{-61.9\,(58.8)}{N + 58.8} = \frac{-3640}{N + 58.8}$$

Numerical values for isoclines in this region are tabulated in Table II.

(2) When both the amplifier and the comparator are in full saturation, $K_a = 133.3$, and no matter what the value of the true error, the plant sees only a constant error of $3.22 \times 10^{-3}$ radians (.6 volts, rms), and:

$$\dot{E} = \frac{23.6\,(58.8)\,E_{const.}}{N + 58.8} = \frac{1385\,(\pm 3.22 \times 10^{-3})}{N + 58.8} = \frac{\pm 4.46}{N + 58.8}$$

In this region the isoclines are parallel to the E axis; numerical values are tabulated in Table III.

Figure 21, the phase plane, was constructed from Tables II and III. Note that there is a transition region between $\pm 3.22 \times 10^{-3}$ and $\pm 1.075 \times 10^{-3}$ radians, where the isoclines are continually changing direction instead of linear because here amplifier gain is continually changing. Note also that for greater figure clarity, the $\dot{E}$ axis, and the corresponding

Table II
Numerical Values of Isoclines in Linear Region
$E < 1.075 \times 10^{-3}$ radians

| $N$ | $\dot{E}/E = -3640/N + 58.8$ |
|---|---|
| +1761.2 | − 2.0 |
| + 305.2 | − 10.0 |
| + 123.2 | − 20.0 |
| + 32.2 | − 40.0 |
| 0.0 | − 61.9 |
| − 5.0 | − 67.7 |
| − 10.0 | − 74.6 |
| − 20.0 | − 93.9 |
| − 25.0 | − 107.7 |
| − 30.0 | − 126.4 |
| − 40.0 | − 193.6 |
| − 58.8 | − ∞ |
| − 78.8 | + 182.0 |
| − 98.8 | + 91.0 |
| − 118.8 | + 60.7 |
| − 218.8 | + 22.7 |
| − 422.8 | + 10.0 |
| − 1878.8 | + 2.0 |

Table III
Numerical Values of Isoclines in Fully Saturated Region
$E \geq 3.22 \times 10^{-3}$ radians

| $N$ | $\dot{E} = \pm 4.46/N + 58.8$ |
|---|---|
| 0 | ± $76.0 \cdot 10^{-3}$ |
| − 5.0 | $82.9 \cdot 10^{-3}$ |
| − 10.0 | $91.4 \cdot 10^{-3}$ |
| − 15.0 | $101.8 \cdot 10^{-3}$ |
| − 20.0 | $115.0 \cdot 10^{-3}$ |
| − 25.0 | $132.0 \cdot 10^{-3}$ |
| − 30.0 | $156.0 \cdot 10^{-3}$ |
| − 32.0 | $166.5 \cdot 10^{-3}$ |
| − 34.0 | $179.9 \cdot 10^{-3}$ |
| − 36.16 | $197.0 \cdot 10^{-3}$ |

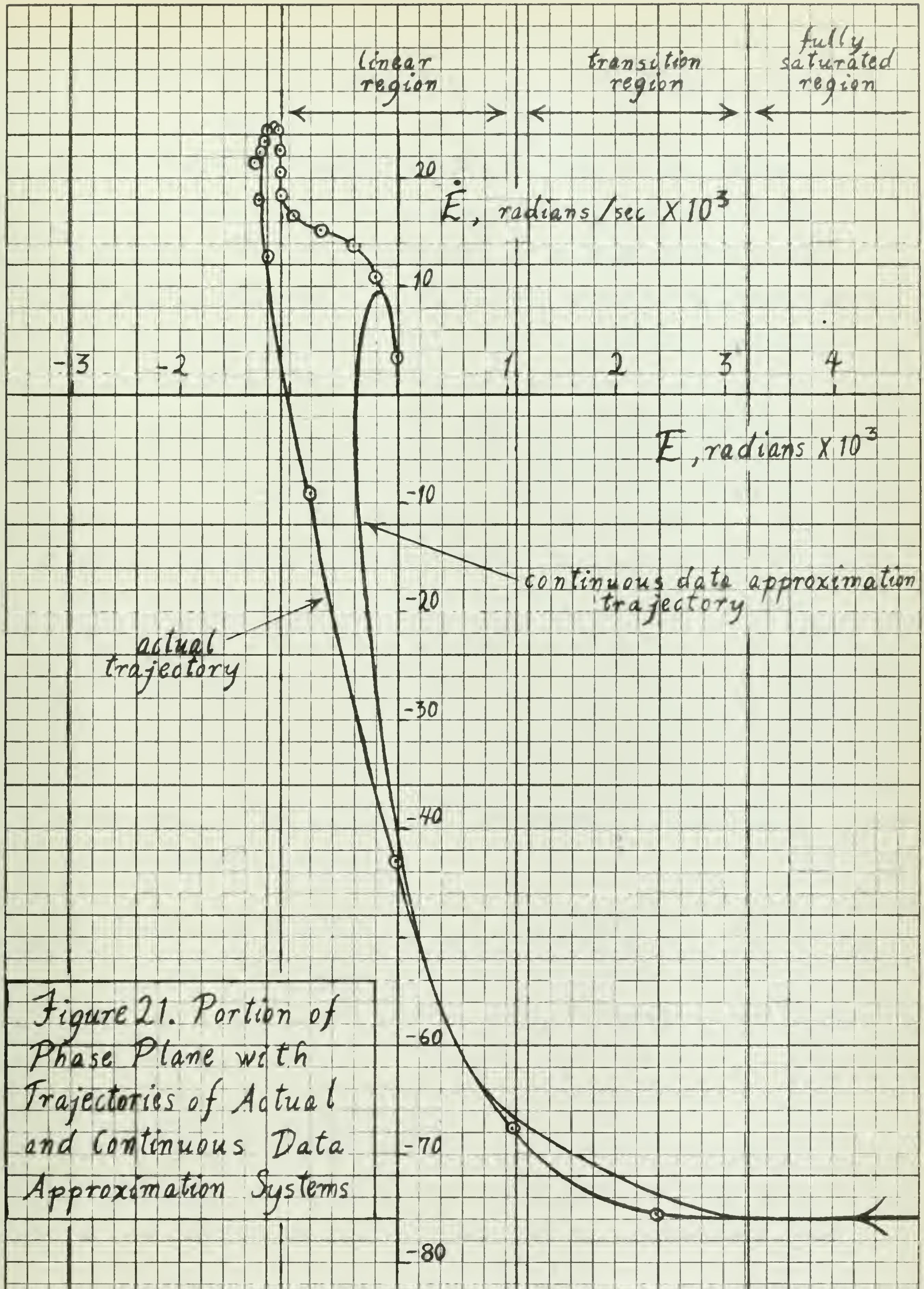


Figure 21. Portion of Phase Plane with Trajectories of Actual and Continuous Data Approximation Systems

values of N have been scaled down by 10 in Figure 21, and the isoclines themselves have not been shown.

A phase trajectory for any step input large enough to push the motor into its velocity limit is shown, together with an actual trajectory derived from Brush Recorder Data.

It is notable that the continuous data trajectory is not too bad an approximation of the true sampled data trajectory. It should be kept in mind that for simplicity's sake the theoretical analysis has not considered the great amount of backlash present, which can be seen quite clearly in the true trajectory. There is a peculiar slight overshoot in the true trajectory before the constant error flat portion typical of backlash; however, this agrees with the transient shown in Figure 19. Note also that the two trajectories are very close together in the early portions. Of course, there is a greater overshoot in the true trajectory, but this is a function of the sampling where the motor does not see the true error but a staircase approximation with its inherent time delay, causing greater overshoot.

### 6.3 Phase Plane Analysis of Dual Mode System

It seems reasonable that using the continuous data approximation of the real system, a dual moding arrangement can be arrived at.

As stated in Section III, it was observed that without rate feedback a maximum velocity of $197 \times 10^{-3}$ radians/sec is attained, and with the proper amount of rate feedback a maximum velocity of $76 \times 10^{-3}$ radians/sec is attained. Thus,

when switching in the rate feedback a sudden, large deceleration is applied. Considering the narrowness of the unsaturated zone in Figure 21, it is quite evident that the rate feedback would have to be switched in before the error is reduced to $\pm 3.22 \times 10^{-3}$ radians to allow the system sufficient time to decelerate a great deal before coming out of saturation. For practical reasons, to be stated later, it was found very convenient to cause the servo to switch modes when the error is $\pm 4.73 \times 10^{-3}$ radians.

Figure 22 is another phase plane plot for the continuous data approximation of the stable rate feedback damped system, showing a trajectory for initial conditions of $E = + 4.73 \times 10^{-3}$ radians and $\dot{E} = -197 \times 10^{-3}$ radians/second. Note again that for clarity, the $\dot{E}$ axis and the corresponding values of N, have been scaled down by a factor of 20 in Figure 22, and the isoclines are not shown.

In comparing theoretical trajectories of Figure 21 with Figure 22 note that although in the dual mode case the servo comes out of comparator saturation ($3.22 \times 10^{-3}$ radians) with almost twice the velocity as previously, it still comes into correspondence with only one more slight overshoot. This indicates the system has a great deal of natural, or inherent damping. This is not surprising if the roots of the characteristic equation are examined. For this continuous data approximation of the sampled data system, in the linear region around the null, the characteristic equation is:

$$s^2 + 58.8s + 3640 = 0$$

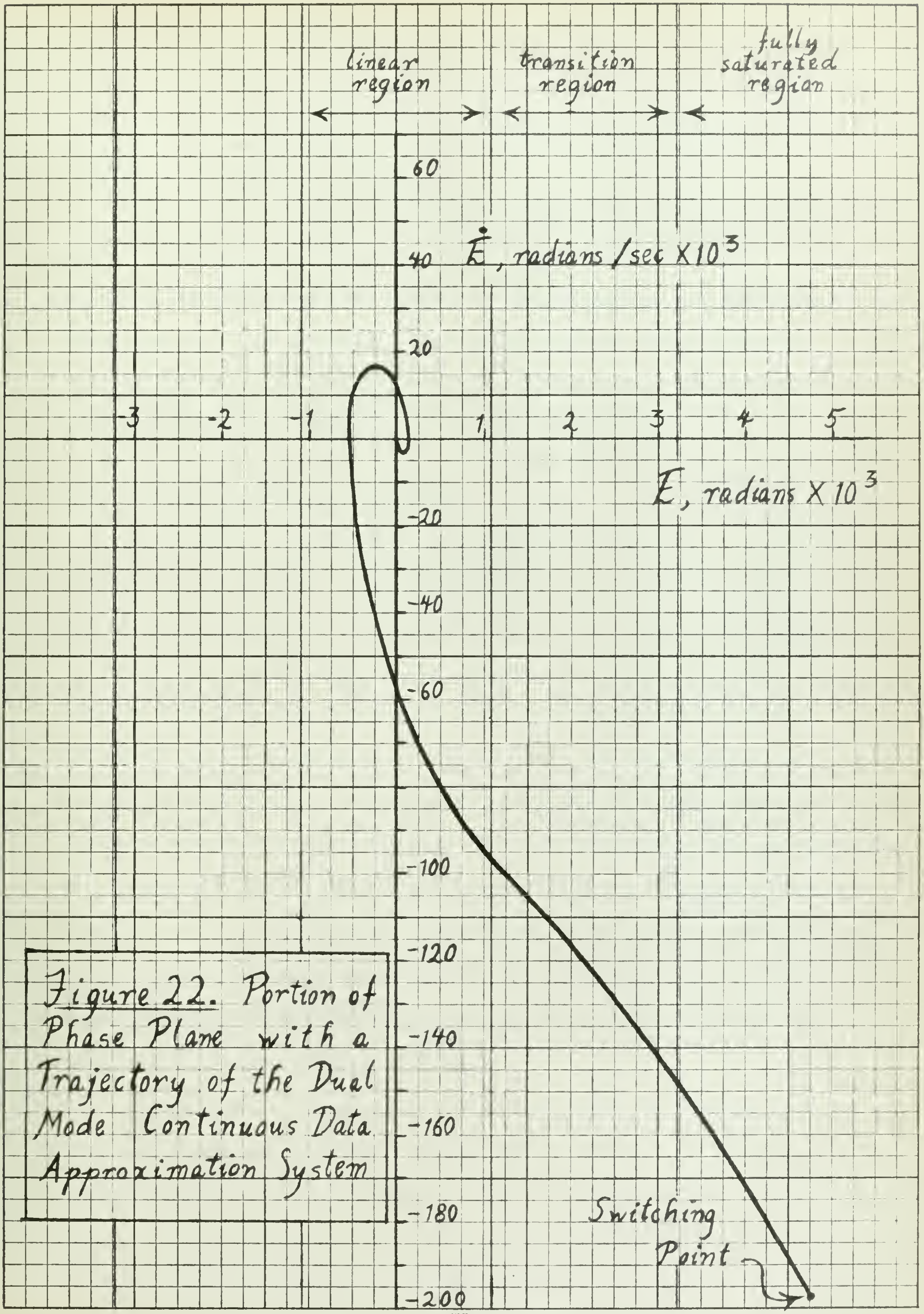


Figure 22. Portion of Phase Plane with a Trajectory of the Dual Mode Continuous Data Approximation System

In the transient, the sine wave resulting from the complex pair roots of this equation are damped by a factor of $e^{-29.4t}$; thus, it is heavily damped.

With this in mind, it was felt that the dual mode arrangement would work in spite of the greater overshoot of the true sampled data system, an effect of the sampling as mentioned previously. The actual system does exhibit this inherent damping in both the transient and on the phase plane where there is a large, but only one-sided overshoot.

### 6.4 Dual Mode Switching Device

Very often in designing a switching device for dual mode operation of a servo one could expect to run into great complication. However this was not the case in this instance. In fact, the design was quite simple, as will be shown. The reason for this was basically that the system being dual-moded is one employing digital devices, in particular, a digital comparator. The Norden-Ketay Digital Comparator employs transistor switches in logical circuitry for performing the algebraic addition of two binary numbers, as explained in Section II. It was found that parts of this same digital circuitry could be used to activate the switching in, or switching out of rate feedback in the system, without interfering in its primary comparison function.

As was shown in the last section, what is needed is a switching device that will hold rate feedback out of the system while the comparator is in its limit, and will put it into the system just before the comparator comes off its

limit. After studying the logic circuitry of that section of the comparator called "Logic Circuits" in Figure 4, two particular points, referred to hereafter as points $A_1$ and $A_2$, were found which jointly could perform a decision function in the desired dual mode switching device. (For convenience in the discussion that follows the magnitudes of error signals will be used in their binary equivalent in the system. For example, an error of $\pm 3.22 \times 10^{-3}$ radians is equivalent to $2^5$, or 32 "bits".) Points $A_1$ and $A_2$ have the following voltage level characteristics in the comparator:

Table IV Voltage Levels of Dual Mode Switching Circuit Decision Function.

| Points | System Input | Error > 47 bits | Error ≤ 47 bits |
|---|---|---|---|
| $A_1$ | Positive Step | -11 | -11 |
| $A_2$ | " | 0 | -11 |
| $A_1$ | Negative Step | 0 | -11 |
| $A_2$ | " | -11 | -11 |

Using the voltages in Table IV, a transistor switching circuit was designed as shown in Figure 23, with pertinent voltage levels under various conditions tabulated in Tables V and VI.

The four 2N344 transistors used in this circuit are P N P type transistors. In order to understand the operation of the circuit it is well to keep the following facts about transistor switches in mind (9):

1. No current (except a small leakage current) will flow in the collector unless current is introduced into the emitter.

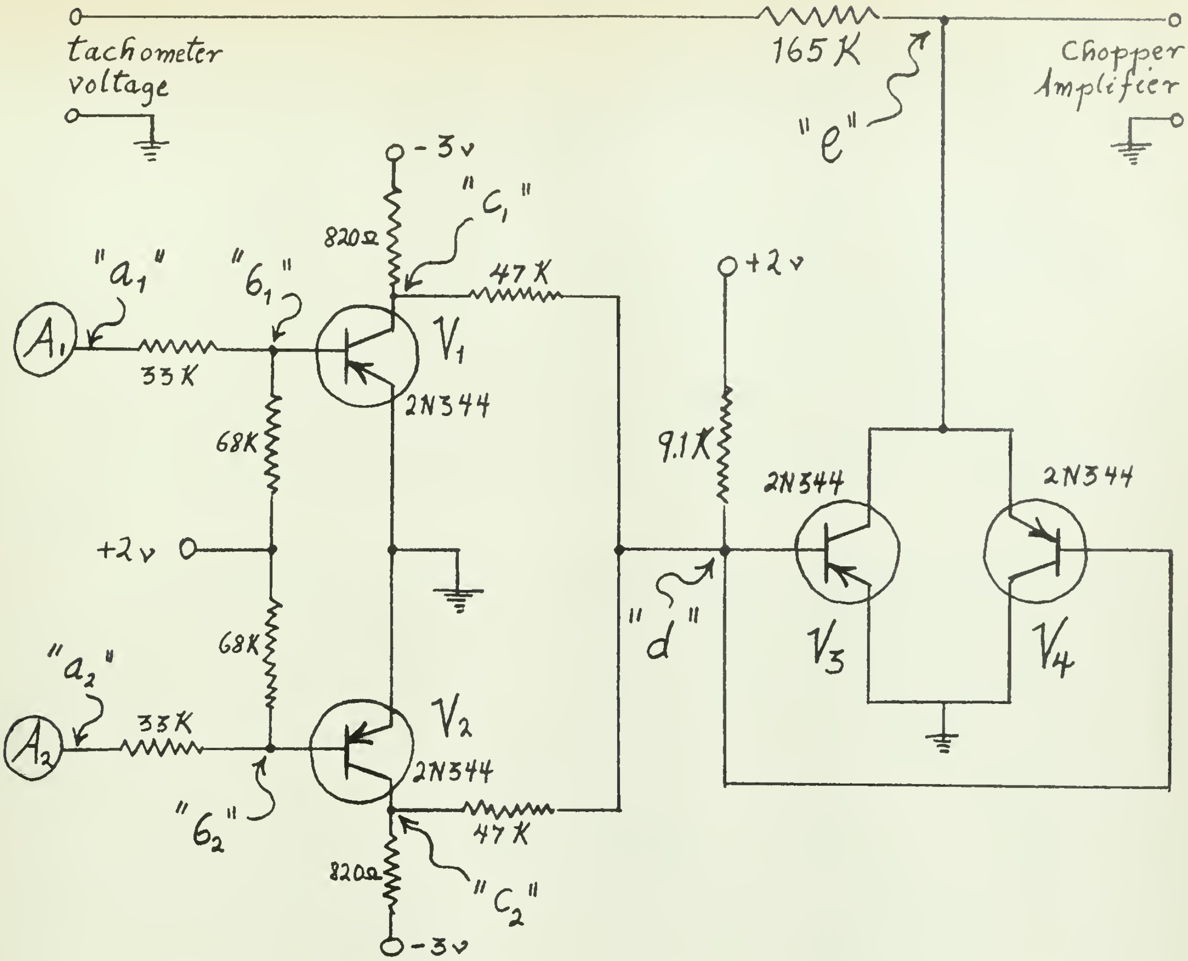


Figure 23. Dual Mode Switching Circuit

| Table V<br>Pertinent Voltage Levels for Positive Step Inputs | | |
|---|---|---|
| Point | E > 47 bits | E ≤ 47 bits |
| $a_1$ | -11 | -11 |
| $a_2$ | 0 | -11 |
| $b_1$ | -0.3 | -0.3 |
| $b_2$ | +0.5 | -0.3 |
| $c_1$ | -2.2 | -0.35 |
| $c_2$ | -0.35 | -0.35 |
| d | -0.2 | +0.22 |
| e | +0.02 | variable |

| Table VI<br>Pertinent Voltage Levels for Negative Step Inputs | | |
|---|---|---|
| Point | E > 47 bits | E ≤ 47 bits |
| $a_1$ | 0 | -11 |
| $a_2$ | -11 | -11 |
| $b_1$ | +0.5 | -0.3 |
| $b_2$ | -0.3 | -0.3 |
| $c_1$ | -0.35 | -0.35 |
| $c_2$ | -2.2 | -0.35 |
| d | -0.2 | +0.22 |
| e | -0.02 | variable |

2. If the base to emitter is back biased by more than .2 volts, the transistor is effectively an open circuit. For a P N P transistor back biasing is achieved when the base is positive with respect to the emitter.

3. If the base to emitter is forward biased, the transistor conducts heavily and is effectively a short circuit.

For example, consider a very large positive step input to the servo. Referring to Figure 23 and Table V, it can be seen that while the error is greater than 47 bits, $V_1$ conducts but $V_2$ does not. Because of this unbalance between $V_1$ and $V_2$, a negative voltage appears at point d, which forward biases $V_4$, causing it to short the tachometer to ground, and no rate feedback enters the servo system. Note, $V_3$ does not conduct although its base to emitter is also forward biased because its collector is positive with respect to its emitter and this is not the proper conduction polarity for a P N P transistor. This situation would be just reversed for a negative step input when the tachometer voltage is negative; then $V_3$ and not $V_4$ would short out the tachometer.

When the error is less than, or equal to 47 bits the unbalance between $V_1$ and $V_2$ is restored because both equally conduct, since $A_1$ and $A_2$ are both −11 volts as shown in Table IV. Therefore, point d becomes positive, which back biases $V_4$ and $V_3$, the short to ground is opened, and rate feedback enters the system.

This switching device worked as designed, and the servomechanism operated successfully in the dual mode arrangement, for all sizes of input signals.

Thus, in this instance, continuous data phase plane analysis gave a good enough approximation of a sampled data system to permit using the technique of dual moding to raise the saturation velocity of the system.

## VII CONCLUSIONS

As stated in the Introduction, the purpose of this investigation was to analyze an existing digital sampled data position servomechanism which is velocity limited, and, further, to find a means of raising the maximum velocity if possible.

From the analysis presented the following conclusions may be drawn:

1. The system studied is a Type 1, second order digital sampled data servo which has no region of linear operation. The predominant nonlinearities are: (a) an error limit imposed by the physical construction of the digital comparator; (b) servo amplifier saturation, (both of which cause the system to be saturated for all but very small input signals); and (c) a large amount of backlash in the 1800:1 gear train.

2. The system achieves its maximum velocity during saturation as a single loop, unity feedback system with no rate feedback, but in this condition it is unstable, resulting in a limit cycle. This instability is the result of an amplifier gain which puts the system roots outside the unity circle, (stability limit), on the z-plane, but this particular amplifier gain is necessary for the servo to respond to a one bit input signal, such performance being required by the design specifications.

3. This velocity limited servo can be made stable for all step inputs of one bit or greater by the addition of an

inner loop consisting of rate feedback around the motor and servo amplifier, but in this arrangement the maximum motor speed, or velocity limit, is reduced. Because of this lowered velocity limit, the time of response for all large inputs which cause saturation is very long.

4. In the stable, rate feedback damped arrangement this system has a great amount of inherent damping. For this reason, the large backlash in the gear train does not constitute an additional source of limit cycles.

5. In order to raise the maximum velocity attained during saturation, dual mode operation proved feasible by neglecting the backlash, and using phase plane analysis with a continuous data approximation of the actual sampled data system. The successful use of this approximation was due principally to the great inherent damping present in the actual system as a result of the rate feedback.

6. A simple dual mode switching device can be designed for this digital system using transistor switches by taking advantage of the existing logical circuitry in the digital comparator. By the use of this switching device the inner loop of the servomechanism is open circuited by large input signals, allowing the system to run at near maximum motor speed until the system position error is very small, at which time the switching device closes the inner loop, putting rate feedback damping into the system to bring it into correspondence without a limit cycle.

BIBLIOGRAPHY

1. "Model A9SP16 9 inch Diameter 16-Digit Shaft Angle Analog-to-Digital Encoder", Industrial Products Division, Baldwin Piano Co., 1958.

2. "Norden Ketay Digital Comparator", Norden Ketay, Data Systems Division, 1958.

3. W. A. Stein and G. J. Thaler, "Evaluating the Effect of Nonlinearity in a 2-phase Servomotor"; Trans. AIEE, Applications and Industry, Jan. 1955.

4. J. R. Ragazzini and G. F. Franklin, Sampled Data Control Systems, McGraw-Hill Book Co., 1958.

5. G. J. Thaler, Lecture notes for a course in Sampled Data Control Systems, U.S. Naval Postgraduate School, 1959.

6. H. Chestnut and R. W. Mayer, Servomechanisms and Regulating System Design, Vol. II, John Wiley & Sons, 1955.

7. R. L. Hovious, "Jitter in Instrument Servos," Trans. AIEE, Applications and Industry, Jan. 1955.

8. R. C. H. Wheeler, Lecture notes for a course in Nonlinear Servomechanisms, U.S. Naval Postgraduate School, 1959.

9. General Electric Transistor Manual, 3rd Ed., General Electric Co., Semiconductor Products Division, 1958.

# APPENDIX I

## GRAY BINARY CODE

In the true, or natural binary number system the normal sequence is shown in Figure 1 below, with the decimal equivalent of the true binary number to the right. As can be seen, often more than one binary digit changes at a time, such as in the decimal equivalent numbers 2, 4, 6, 8.

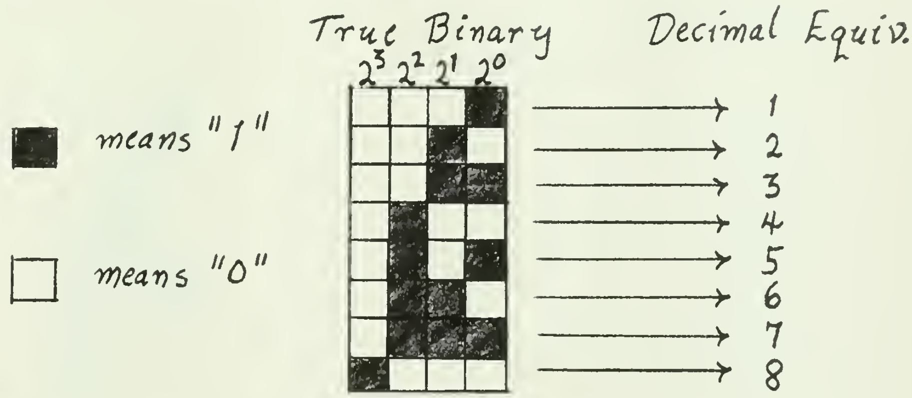


Figure 1. True Binary Counting Sequence

The Gray Binary Code, named for its inventor, Dr. Frank Gray, was devised in order to minimize serious reading error in digital equipment by allowing only one binary digit to change at a time. At the left in Figure 2 is the Gray Binary counting sequence, where this fact can be readily seen.

To convert the Gray Binary sequence to the true binary sequence, for each number in Gray Binary simply add the digits, starting from the most significant and working progressively toward the least significant as follows:

First: Carry the most significant digit unchanged.

Second: Add the most significant digit to the second

most significant digit, the result is the true binary second most significant digit. In this addition 1 + 0 = 1, and 1 + 1 = 0.

Third: Take the result of the second step, (the true binary second most significant digit), and add it to the third most significant Gray binary digit, the result is the true binary third most significant digit, etc.

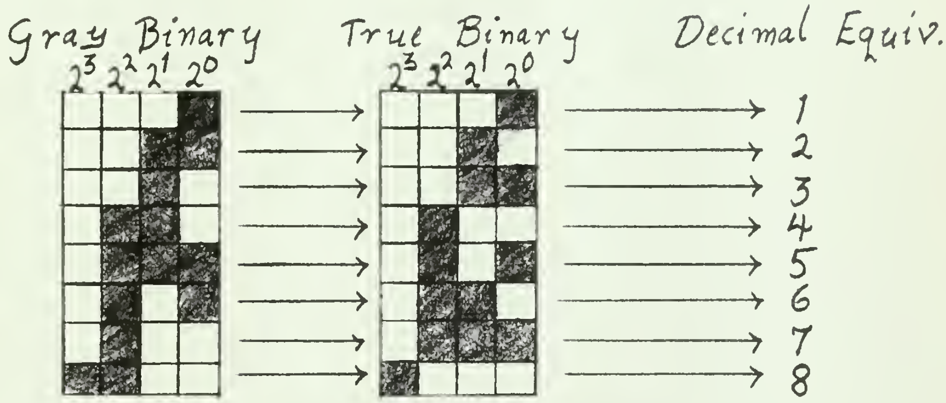


Figure 2. Comparison of Gray Binary Numbers and Their True Binary Equivalents

Referring to Figure 2, some examples of conversion follow, using an arrow sequence to signify the addition steps above:

| | | | | | | | | | |
|---|---|---|---|---|---|---|---|---|---|
| Gray binary: | 0 | 0 | 1 | 1 | | 1 | 1 | 0 | 0 |
| True binary: | 0 | 0 | 1 | 0 | | 1 | 0 | 0 | 0 |

thesB5458
An analysis of a digital sampled data se
3 2768 002 13520 4
DUDLEY KNOX LIBRARY